Precambrian Research 383 (2022) 106902

Contents lists available at ScienceDirect

Precambrian Research

journal homepage: www.elsevier.com/locate/precamres

Oxygen-induced chemocline precipitation between Archean Fe-rich and Fe-poor carbonate seas

Robert Riding [a,*], Liyuan Liang [a], Philip Fralick [b]

[a] Department of Earth and Planetary Sciences, University of Tennessee, Knoxville, TN 37996-1526, USA
[b] Department of Geology, Lakehead University, Thunder Bay, Ontario P7B 5E1, Canada

ARTICLE INFO

Keywords:
Archean
Canada
Carbonate
Oxygenation
Seawater

ABSTRACT

The removal of dissolved iron by oxygen was a key control on marine Ca-carbonate precipitation during the Archean, but many details remain poorly resolved. We examined thick carbonate platforms, ~2.9–2.8 Ga, in the western Superior Province of Canada. Interlayered Fe and Ca-carbonate minerals suggest platform margin precipitation, both as seafloor crusts and in the water column, during mixing of anoxic offshore and oxygenated onshore water masses in dynamic chemoclines. Platform interiors were subject to short-lived influxes of Fe-rich anoxic offshore waters that variously precipitated aragonite, herringbone calcite, Fe-dolomite, and rare siderite. Overall, these observations are consistent with chemical equilibrium analysis assuming three co-existing confluent carbonate water masses: (i) offshore anoxic iron-rich seawater, precipitating Fe-carbonate, (ii) a chemocline mixing zone variously precipitating interlayered aragonite, calcite and Fe oxide, (iii) onshore iron-poor seawater precipitating calcite and aragonite in an 'Oxygen Oasis'. In this system, Fe^{2+}, at ~ 3 orders of magnitude lower level, supersedes the effect of Mg^{2+} on Ca-carbonate mineralogy. Only when sufficient Fe^{2+} was removed by oxygenation did the relative concentrations of Mg^{2+} and Ca^{2+} determine $CaCO_3$ mineralogy. Platform margin chemoclines created by oxygen production likely persisted throughout the Archean.

1. Introduction

Aragonite ($CaCO_3$), calcite ($CaCO_3$), dolomite ($CaMg(CO_3)_2$), Fe-dolomite ($Ca(Mg,Fe)(CO_3)_2$ and siderite ($FeCO_3$) are common sedimentary carbonate minerals (Lippmann, 1973). Their geological distributions as marine precipitates suggest long-term variations in seawater composition with respect to the relative abundance of Ca, Mg and Fe (Chilingar, 1956; Ronov, 1968; Holland, 1973; Simonson, 1985; Veizer et al., 1989). In present-day seawater, Mg concentrations greater than four times Ca (Lebrato et al., 2020) can slow calcite precipitation, resulting in widespread aragonite (Sun et al., 2015 and references therein). Consequently, the molar Mg/Ca ratio of seawater is one of the factors responsible for the present-day dominance of aragonite and Mg-calcite in bioinduced and abiotic precipitates, particularly in tropical seas (Balthasar and Cusack, 2015). Numerous studies indicate that long-term fluctuations in seawater Mg/Ca contributed to alternating 'Aragonite' and 'Calcite Seas' conditions throughout the Phanerozoic (e.g., Sandberg, 1985; Spencer and Hardie, 1990; Hardie, 1996, 2003; Horita et al., 2002; Lowenstein et al., 2001, 2014; Morse et al., 2007; Bots et al., 2011; Balthasar and Cusack, 2015). During the Proterozoic, it is likely that even higher Mg/Ca may at times have facilitated synsedimentary replacement of aragonite by dolomite, as in the Cryogenian (Hood and Wallace, 2012, 2018).

Published estimates suggest that from the Archean to the present-day, fluctuations in seawater Mg and Ca concentrations have been much less than an order of magnitude (Ries, 2010; Jones et al., 2015). In contrast, estimates of dissolved Fe concentrations for anoxic Archean seas (~1 mM) (Kipp and Stüeken 2017; Song et al., 2017) (Fig. 1) are six orders of magnitude higher than in present-day open surface seawater (<0.2 nM) (De Baar and De Jong, 2001; Boyd and Ellwood, 2010). Such high levels of Fe^{2+} are consistent with widespread occurrence of Fe-carbonate, -oxides, -silicates and -sulfides in marine sedimentary iron formation during the Archean (Dymek and Klein, 1988; Bekker et al., 2010). At ~ 1 mM Fe^{2+} concentration, Ca-carbonate mineral precipitation is inhibited and siderite ($FeCO_3$) would be the carbonate mineral to precipitate (Klein and Beukes, 1989; Sumner, 1997a; Canfield, 2005). Laboratory studies show that - depending on factors such as pH, the valance state and concentration of iron, the presence of O_2, and the saturation state (Ω) of $CaCO_3$ minerals - Fe strongly inhibits calcite, but not aragonite (Herzog et al., 1989; Katz et al., 1993). Consequently, in

* Corresponding author.
E-mail addresses: rriding@utk.edu (R. Riding), lliang1@utk.edu (L. Liang), pfralick@lakeheadu.ca (P. Fralick).

https://doi.org/10.1016/j.precamres.2022.106902
Received 15 April 2022; Received in revised form 19 September 2022; Accepted 31 October 2022

Archean seawater, (i) Ca-carbonate minerals should only have precipitated if Fe^{2+} were locally scarce or had been removed by oxidation (Klein and Beukes, 1989; Sumner, 1997a; Canfield, 2005), and (ii) progressive Fe-removal can be expected to have led first to aragonite and then calcite precipitation. Thus, if Archean seas were generally Fe-rich and anoxic (Canfield, 2005; Holland, 2006; Kipp & Stüeken, 2017), the sedimentary precipitation of Ca-carbonate minerals could be regarded as an indicator of localized, but relatively sustained, iron removal and perhaps oxygenation (Riding et al., 2014; Fralick & Riding, 2015).

Relationships between Fe-rich seawater and oxygenation are central to deciphering the rock record of Archean marine carbonates. Many uncertainties remain. It is especially important to recognize sediments that reflect changes in carbonate mineralogy associated with possible steep oxygen gradients or other means of precipitating iron-bearing minerals. Here we describe adjacent Fe-rich and Fe-poor sediments located at the seaward margins of two mid-Archean (~2.9–2.8 Ga) carbonate platforms in central Canada.

2. Southern Superior Province, Canada, ~2.9–2.75 Ga

Mesoarchean oceanic volcanic plateaus are common in the Western Superior Province of Canada (Hollings and Wyman, 1999; Hollings et al, 1999; Fralick et al., 2008), whereas volcanic arcs dominated during the Neoarchean (Thurston and Chivers, 1990; Percival et al., 2012; Thurston, 2015), with collisions between them beginning ~ 2.72 Ga in northern Superior Province and the craton accreting to the south until ~ 2.68 Ga (Langford and Morin, 1976). In this region, marine chemical sediments – mainly chert, iron formation and Ca-carbonates – accumulated during intervals of locally reduced volcanism (Thurston and Chivers, 1990; Percival et al., 2012; Thurston et al., 2012; Thurston, 2015). These include relatively thick (≥200 m) Ca-carbonate platforms at Red Lake (~2.94 Ga) and Steep Rock Lake (2.80 Ga), and locally extensive basinal Fe-carbonate deposits, e.g., at Wawa (~2.75 Ga) (Fig. 2).

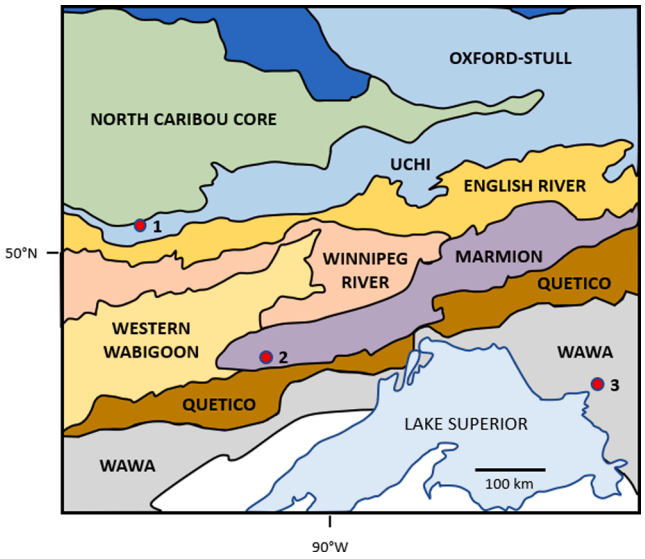

Fig. 2. Geological domains of the western Superior Province, Canada (after Stott et al., 2010) showing general locations of Red Lake (1) and Steep Rock Lake (2) carbonate platforms, and Wawa siderite (3).

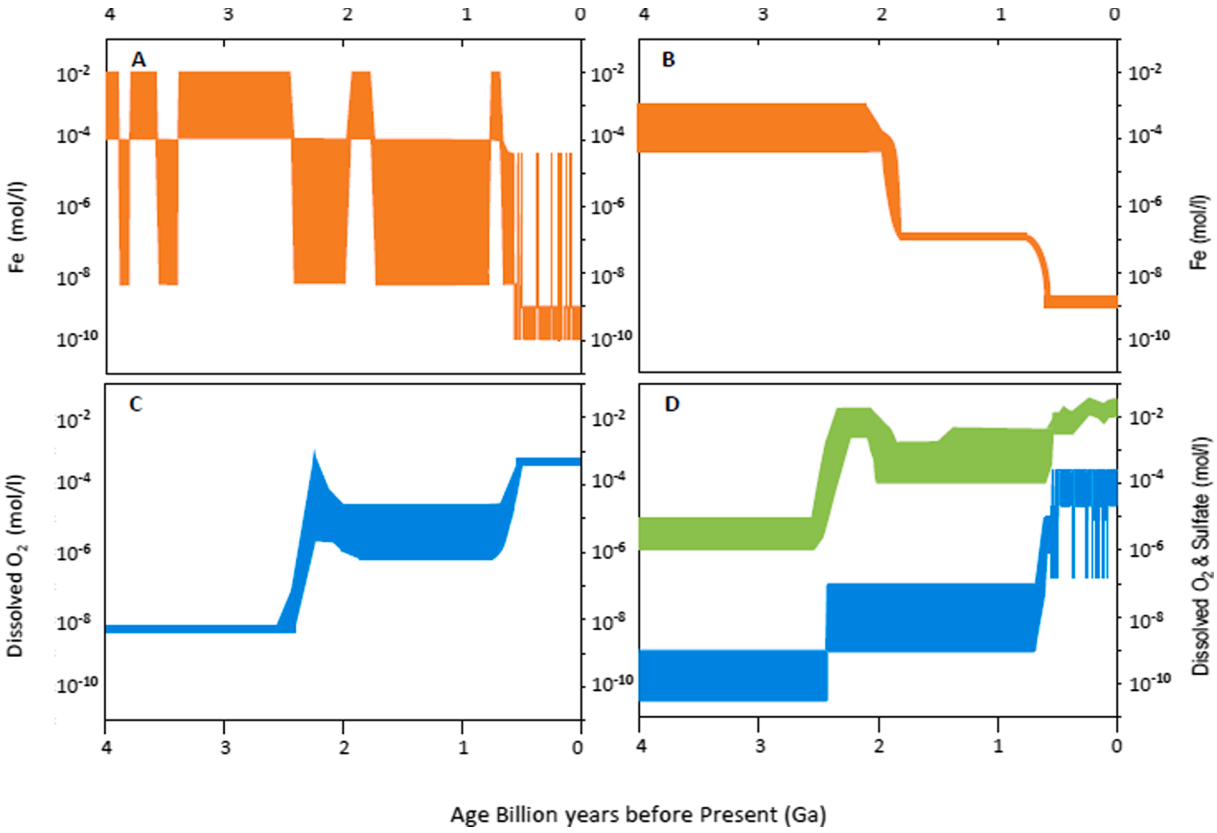

Fig. 1. Estimates of long-term trends in seawater ionic composition. A. Fe (Song et al., 2017, fig. 2d). B. Fe (Kipp and Stüeken 2017, fig. 1a). C. Dissolved O_2 (Kipp and Stüeken 2017, fig. 1a). D. Dissolved O_2 (blue) (Song et al., 2017, fig. 2e) and sulfate (green) (Kipp and Stüeken 2017, fig. 1a). (For interpretation of the references to color in this figure legend, the reader is referred to the web version of this article.)

2.1. Red Lake carbonate Platform, ~2.94–2.92 Ga

2.1.1. Geologic setting and age

Red Lake carbonate platform (Hofmann et al., 1985; McIntyre and Fralick, 2017, Fig. 2) is located ~ 450 km north-west of Thunder Bay, Ontario, in the Red Lake Greenstone Belt (Uchi Subprovince, western Superior Province) (Sanborn-Barrie et al., 2000, 2001; Satkoski et al., 2017) (Fig. 2). In this area, ~25 km west of Red Lake town, sub-vertical south-younging carbonates and associated sediments occur in a gently arcuate east–west zone up to ~ 0.5 km wide and ~ 11 km in length (Sanborn-Barrie et al., 2004). This ~ 200-m thick succession of limestones and dolostones with intercalated sandstones, organic-rich slates, chert and both oxide and sulfide iron formation, occurs between underlying sandstones and overlying basalts of the Ball Assemblage (Afroz, 2019). These deposits indicate a coherent platform, ~200 m thick and at least ~ 10 km in lateral extent, that may originally have been contiguous with similar lithologies at Wallace Lake, 100 km to the west (Hofmann et al., 1985; McIntyre and Fralick, 2017). U-Pb age determinations on underlying and overlying rhyolites constrain the age of the carbonates to ~ 2.940–2.925 Ga (Corfu and Wallace, 1986; Thurston et al., 1991).

2.1.2. Lithologies and environments

Red Lake carbonates are chert-bearing limestones and dolostones that become more calcitic seaward, locally with horizons of crystal crust interpreted as originally aragonite (McIntyre and Fralick, 2017). Carbonate microfabrics are generally recrystallized and macroscopic fabrics range from poorly to well preserved. Although neomorphism obscures the original grain-size, homogeneous, mainly planar, banded fabrics ('ribbon rock') typical of carbonate mud deposits are common (Riding et al., 2020). Conspicuous fabrics include fenestral-crenulate crinkly crust (Afroz, 2019, fig. 3.1b), thin radial acicular crystal crust (atikokania) (Fig. 3) and stromatolitic units (McIntyre & Fralick, 2017, fig. 4). The latter include small to medium-size irregular to steep sided domes and pseudocolumns (Hofmann et al., 1985) and less common bulbous forms. Rare, but distinctive, fabrics include meter-size radial domes of crystal crust interpreted as originally aragonite (Fig. 4) and beds of herringbone calcite (Fig. 5). Slabbed samples show that meter-scale layered domes at Hahn Lake (51.041036, −94.144788) contain layers of crystal fans. Sequences locally show upward transition from 'ribbon rock' to small domes, fenestral-crenulate crusts and stromatolitic pseudocolumns, consistent with shallowing. Flakestones, flat-pebble breccias and atikokania fragments (Fig. 6) occur occasionally. Planar stromatolites and thin atikokania crust commonly co-occur. Rare gypsum-like pseudomorphs occur in nearshore facies (McIntyre and Fralick, 2017, fig. 3d).

Although definitive depth indicators are scarce, fenestral-crenulate crusts and brecciated crystal crusts locally suggest very shallow water deposition, and the lateral and vertical varieties of lithotypes and stromatolites are consistent with deposition on an extensive shallow-water platform (McIntyre and Fralick, 2017). Negative Ce anomalies have been identified in laminites underlying a crystal fan mound (McIntyre and Fralick, 2017) in the upper part of the succession (Afroz, 2019). Shoreward increase in dolomite and resetting of Sr isotopes (Satkoski et al., 2017) in dolomitized strata, but not in more offshore calcite, suggest early dolomitization of platform interior sediments (McIntyre and Fralick, 2017). At both Red Lake and Steep Rock Lake the calcite consistently has <1 percent Fe, with the dolomite at Red Lake containing <2 percent Fe. The ankerite bands at Steep Rock have larger amounts of Fe^{2+} but these are not volumetrically important. Basalt with

Fig. 3. Crystal fans (atikokania), Red Lake, Ontario. 51°01′52.2″N 94°11′29.0″W.

Fig. 4. Radial crystal fan dome (~1.25 m wide, 0.75 m high), partially silicified, interpreted as originally aragonite. Golden Arm, Red Lake, Ontario. 51°02′54.8″N 94°06′50.6″W.

Fig. 5. Herringbone calcite seafloor crust. Bridget Lake, Red Lake, Ontario. 51°01′49.8″N 94°13′12.2″W.

Fig. 6. Coarse synsedimentary breccia with fragments of crystal crust (atikokania). Red Lake, Ontario. 51°01′55.1″N 94°11′08.3″W.

iron formation overlies the carbonate (Sanborn-Barrie et al., 2004) and iron formation is interbedded with Red Lake carbonates (Hofmann et al., 1985) in units up to 10 m thick, but mainly < 1 m thick (Fig. 7) (McIntyre and Fralick, 2017). Pronounced Eu anomalies indicate that the iron minerals precipitated from seawater with the majority of rare earth elements derived from hydrothermal circulation (Afroz, 2019). An increase in MnO_2 content, from 0.94 to 4.10 percent, was observed in the iron formation with increasing proximity to the carbonate platform (Afroz, 2019).

Transition to platform margin/slope conditions may be indicated by evidence of soft-sediment deformation and slumping; e.g., brecciated and slumped cherty carbonate layers associated with iron formation at Hall Bay (51.035463, −94.146610) ~ 24 km west of Red Lake town (McIntyre and Fralick, 2017, fig. 7c; Afroz, 2019, fig. 33). At this locality, a ~ 0.5 m intercalation of alternating thin layers of fine-grained Ca-carbonate and magnetite with a thickness ratio of ~ 5:1–6:1 are underlain by slump deposits (Afroz, 2019) (Fig. 8). In addition, horizons of herringbone fabric (named by Sumner and Grotzinger, 1996a) (Fig. 5), extensive atikokania crusts (originally aragonite) (Fig. 3) and local development of large radial crystal fan domes (originally aragonite) (Fig. 4), suggest incursions of offshore Fe-rich water of variable, but mostly short-lived, duration into the platform interior (see Discussion). In the absence of clear evidence for high energy platform margin conditions, these facies intercalations could be consistent with either ramp or rim geometries, or combinations of both, during much of Red Lake platform accretion.

2.2. Steep Rock Lake carbonate Platform, ~2.8–2.78 Ga

2.2.1. Geologic setting and age

Steep Rock Lake carbonate platform in the Wabigoon sub-province, 200 km WNW of Thunder Bay, Ontario, consists of Mosher Carbonate (Wilks and Nisbet, 1988) which, together with the underlying Wagita sandstone-conglomerate Formation (Wilks and Nisbet, 1988), unconformably overlies tonalitic gneiss of the Marmion Complex (3003 ± 5 Ma, Davis and Jackson, 1988; 3003 ± 3 Ma, Tomlinson et al., 1999; 3001.6 ± 1.7 Ma, Tomlinson et al., 2003). The Mosher is conformably overlain by ~ 200 m of iron formation containing chert, magnetite, carbonaceous pyritiferous slate and minor Fe-dolomite layers (Fralick & Riding, 2015). The iron formation contains up to 19 % MnO_2 adjacent to the Steep Rock platform, but this declines offshore to <0.5 % MnO_2 (Huston, 1956). The maximum age of the Mosher is constrained at 2828 ± 1 Ma (Tomlinson et al., 2003) by the youngest age of underlying volcanics. Pyroclastics overlying the iron formation are 2780.4 ± 1.4 Ma (Tomlinson et al., 2003). A sample of Wagita sandstone with a youngest zircon of 2779 ± 22 Ma (Denver Stone, pers. comm.) places the basal unit of the Steep Rock Group as probably younger than 2801 Ma. Thus, the estimated age of the Mosher is 2.80–2.78 Ga (Fralick & Riding, 2015). The Mosher can be traced discontinuously for at least 50 km. Despite localized replacement by Fe-dolomite, much of the carbonate is preserved as limestone with generally thin bands of Fe-dolomite and dolomite (Fralick & Riding, 2015). Carbonate microfabrics are largely recrystallized (Wilks and Nisbet, 1988), but macrofabrics are locally well-preserved.

Fig. 7. Iron Formation, Red Lake, Ontario. Vertical dip. Eastern side of Bow Narrows, ~2 km west of Hall Bay. 51°02′02.6″N 94°10′25.6″W.

Fig. 8. Ca-carbonate and intercalated magnetite layers, with thickness ratio ~ 5:1–6:1, Hall Bay, Red Lake, Ontario. These repeated centimetric-millimetric intercalations of carbonate mud (light gray) and thin magnetite layers (dark gray) are interpreted as alternating oxygen-induced chemocline water column precipitates. Centimeter scale. Rotated image, original dip is near-vertical. 51°02′07.9″N 94°08′48.4″W.

2.2.2. Lithologies and environments

At Steep Rock Lake, 6 km north of Atikokan town, the Mosher is divisible into the lower ≥ 120-m thick Hogarth Member and upper ≥ 70-m thick Elbow Point Member (Fralick & Riding, 2015, fig. 5). The Hogarth consists largely of relatively fine-grained, thin-bedded limestone with a variety of domal, pseudocolumnar, columnar and stratiform stromatolites. Meter-scale 'ribbon rock' domes, locally with sheet cracks and stromatactis-like fabrics, occur in the upper part. The Elbow Point Member, virtually entirely composed of innumerable juxtaposed, elongate, meter-scale 'Giant Domes' that are evenly and moderately thickly layered (Fig. 9), is interpreted as shallow current-swept platform margin facies, and the Hogarth is interpreted as platform interior (Fralick and Riding, 2015). It is also possible that the lower Hogarth had ramp geometry during transgression over the exposed tonalite terrain. Overall, the Mosher has been interpreted as a shallow, oxygenated, isolated marine carbonate platform subject to short-lived incursions of offshore Fe-rich anoxic water (Riding et al., 2014; Fralick & Riding, 2015).

The Hogarth and Elbow Point members both contain lithologies with mineral layering that can be interpreted as iron-incursion influenced banding (See Section 3.4). In the Hogarth Member these include (i) stromatolite domes with layers of Fe-dolomite and (ii) thin Fe-dolomite intercalations within occasional atikokania radial crystal fan horizons (interpreted as originally aragonite). As at Red Lake, the latter suggest episodic incursions of Fe-rich offshore water into platform interior environments. (iii) The Elbow Point Member is dominated by thick to thinly banded Giant Domes with alternating layers of calcite and calcite pseudomorphs after aragonite (Fralick and Riding, 2015).

(i) Banded nearshore domical stromatolites

Nearshore limestones overlying eroded tonalite in the lower 10 m of the Hogarth Member (Locality 1, Fralick and Riding, 2015, supplemental data) contain a 30 cm stromatolite biostrome (Wilks and Nisbet,

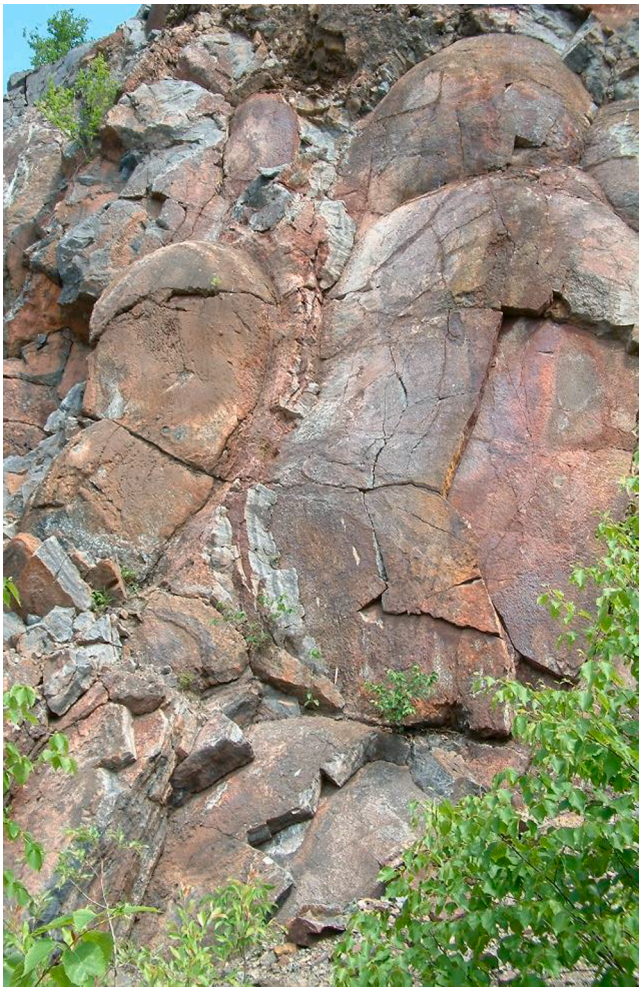

Fig. 9. Steeply dipping layered hybrid Giant Domes interpreted as platform margin chemocline precipitates. Light gray bands are cuspate fenestral fabric, dark gray bands are calcite seafloor crust interpreted to be after aragonite. Elbow Point Member, Steep Rock Lake, Ontario (locality 2 in Fralick and Riding, 2015, fig. 4a). Width of view ~ 7 m. 48°48′59.0″N 91°38′27.8″W.

Fig. 10. Banded carbonate fabrics, Steep Rock Lake platform interior. Corrugated fabric of stromatolite dome composed of layers of calcite (gray) and Fe-dolomite (brown). Units 1 and 2, basal Hogarth Member (see Fralick and Riding, 2015, fig.5). 48°48′58.6″N 91°38′20.9″W.

1985) formed by numerous small laterally linked low domes and pseudocolumns, ~5 cm across, composed of millimetric alternations of calcite (gray) and Fe-dolomite (brown) (Fralick and Riding, 2015) (Fig. 10).

(ii) Platform interior fine-grained sediments with atikokania

Platform interior limestones that form the basal 30 m of the Hogarth Member at Steep Rock Lake Locality 1 (Fralick and Riding, 2015) are overlain by 30 cm horizons of atikokania crystal fans, which have been interpreted as originally aragonite (Fralick and Riding 2015). In turn, these are overlain by 40 cm of columnar stromatolites composed of Fe-dolomite with minor iron oxides (Fig. 11). This succession, with 30 m of calcite sediment overlain by thin intercalations of calcite pseudomorphs after aragonite and Fe-dolomite with minor iron oxides, suggests episodic incursion of off-shore Fe-rich water into inner platform Fe-poor waters that kinetically suppressed calcite precipitation and deposited first aragonite and then Fe-rich dolomite as the Fe^{2+} content of the water increased (Fralick and Riding, 2015).

(iii) Platform margin Giant Domes

Steep Rock Giant Domes, previously described as stromatolites (Walter, 1983; Wilks and Nisbet, 1985), are distinctively layered hybrid structures (Fralick and Riding, 2015; Kurucz and Fralick, 2018; Riding and Virgone, 2020) and are only partly microbial. On the northern side of Errington Pit (Locality 6 of Fralick and Riding, 2015) individual domes are commonly 2–3.5 m wide and up to 1 m thick (Fig. 12). The domes consist of alternating ~ 2–20 cm thick layers of: 1) dark radial crystal fan fabric, now calcitic but high in Sr, with negative Ce anomalies, interpreted as originally aragonite seafloor crust; 2) pale calcitic cuspate fenestral fabric, also locally high in Sr and with negative Ce anomalies, interpreted as partly microbial; and fenestral fabric that is lower in Sr, which was probably originally calcite, and does not have Ce anomalies. Commonly separating these layers are thin Fe-dolomite and /or Fe-oxide layers (Fig. 13). These interlayered precipitates have Ca-carbonate to Fe-mineral thickness ratios in the range ~ 10:1 to ~ 20:1 (Figs. 12, 13). In addition to negative Ce anomalies, these deposits also contain positive Gd anomalies and small positive Eu anomalies (Fralick & Riding, 2015; Kurucz & Fralick, 2018). Rare earth elements (REEs) in

Fig. 11. Banded carbonate fabrics, Steep Rock Lake platform interior. Thin horizon of atikokania crystal fans, inferred to be originally aragonite, and Fe-dolomite. The crystal fans shown here are (out of view) underlain by laminated carbonate, inferred to be originally calcite, and overlain by stromatolites with significant amounts of Fe-dolomite and hematite. This is interpreted as deposition by influx of offshore anoxic water into oxygenated platform interior carbonates. Compositional inferences based on Sr contents. Located near base of Unit 7, mid-Hogarth Member (see Fralick and Riding, 2015, fig. 5). 48°48′59.4″N 91°38′23.8″W.

Fig. 12. Banded laterally linked Giant Domes. Thin iron carbonate/oxide layers (brown) are visible together with evenly layered dark grey crystal fans (interpreted as originally aragonite), and light gray cuspate fenestral fabric. Thicknesses roughly in the proportion 10:1–20:1 $CaCO_3$ to Fe-oxide minerals. Steep Rock Lake, Elbow Point Member, near Errington Pit (locality 6 in Fralick and Riding, 2015, fig. 4a). Pen scale, lower left center, is 15 cm long. This is part of a 60 m thick Giant Dome unit, interpreted to preserve the interaction of upwelling offshore Fe-rich anoxic deep-water with shallow oxygenated platform water. In this view, oxidative removal of Fe^{2+} precipitated Fe-oxides and facilitated aragonite crust precipitation. With continued Fe^{2+} removal, calcitic stromatolitic 'cuspate fenestral fabric' formed. The original aragonite crust is now calcite but preserves its original fibrous crystal fabric with abundant strontium that preferentially incorporates into aragonite (Fig. 15); it also contains negative Ce anomalies indicating oxygenated water. 48°47′42.7″N 91°38′03.5″W.

Fig. 13. Banded carbonate fabric within a Giant Dome. Steep Rock Lake, Elbow Point Member, near Errington Pit (locality 6 in Fralick & Riding, 2015, fig. 4a). Thick crystal fan fabric (dark gray), interpreted as originally aragonite crust, with cuspate fenestral calcite fabric (pale gray) and thin iron-rich layers (brown). These interlayered precipitates, with thicknesses very approximately in the ratio 20:1 Ca-carbonate to Fe-oxide, are interpreted to reflect progressive oxygenation that successively precipitated Fe-oxide, aragonite and calcite from originally anoxic seawater at the shelf-margin chemocline. 48°47′42.7″N 91°38′03.5″W.

carbonates have been widely used as proxies for seawater composition (e.g., see references in Fralick and Riding, 2015) since REEs are not fractionated during incorporation into microbial carbonates (Webb and Kamber, 2000), or during freshwater diagenesis that can cause extensive neomorphism (Webb et al, 2009), or over extended periods of diagenesis (Nothdurft et al., 2004).

3. Discussion

The presence of Fe in Late Archean seawater has been linked to preferential precipitation of aragonite and herringbone calcite seafloor crusts, as well as to the scarcity of water column micrite, at platform margins (Sumner and Grotzinger, 1996a; 2004; Sumner, 2002). More broadly, Riding et al. (2014) hypothesized that Ca-carbonate precipitation in shallow water adjacent to Fe-rich seas could suggest that Archean carbonate platforms, as a whole, represent Oxygen Oases localized by oxygenic photosynthesis beside anoxic iron-rich basins. If this is the case, it could be expected that Ca-carbonate precipitation was initiated by mixing of adjacent confluent water masses at platform margin oxygen controlled chemoclines (Fig. 14). Here we explore these possibilities by examining the interlayered precipitates preserved at the margins of the Red Lake and Steep Rock Lake platforms, as well as the sediments within the platform interiors.

The precipitation of Ca-carbonate from seawater on shallow platforms at Steep Rock Lake and Red Lake and coeval precipitation of iron compounds offshore in deeper water highlight the presence of chemoclines separating these areas. Several explanations for the development of these chemoclines can be envisaged. Freshwater runoff from land could have modified nearshore seawater chemistry. However, Steep Rock appears to have been an isolated carbonate platform in which the initial sub-aerially exposed areas were drowned during marine transgression (Fralick et al., 2008). This is supported by the almost complete lack of siliciclastic sediment within Steep Rock and Red Lake carbonates (Fralick and Riding, 2015; McIntyre and Fralick, 2017), consistent with insignificant freshwater runoff from a land mass. We therefore infer that the chemical gradients that developed at the margins of these platforms originated solely in seawater.

Understanding these chemical gradients requires knowledge of the processes that deposited the iron formation. Suggested origins of iron formation include: 1) ultraviolet radiation splitting H_2O and/or CO_2 to provide free oxygen capable of combining with Fe^{2+} in solution, or Fe^{2+} and $Fe(OH)^+$ utilizing ultraviolet radiation to form dissolved ferric iron, which would have hydrolyzed, forming ferric hydroxide (Cairns-Smith, 1978; Braterman et al., 1983); 2) formation of greenalite that was then altered to iron oxides (Rasmussen et al., 2021); 3) iron hydroxides that were metabolic by-products of anoxygenic phototrophic bacteria (Widdel et al., 1993; Konhauser et al., 2002; Kappler et al., 2005; Thompson et al., 2019); 4) the presence of free oxygen produced by oxygenic photosynthesis (Cloud, 1973). An inherent problem with photolysis of H_2O or CO_2 is that the photolysis products recombine (Catling and Claire, 2005). Additionally, the flux of atmospheric hydrogen, derived from igneous activity, would have been two orders of magnitude greater than photolytic O_2 production, making it very

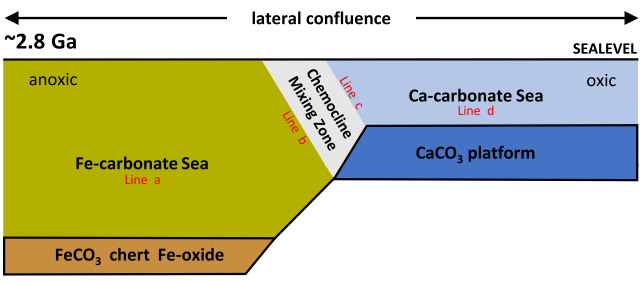

Fig. 14. Interpretive mid-Archean carbonate sea configurations ~ 3.0–2.8 Ga, recognizing laterally confluent carbonate-related water masses (see Section 3.5), based on Red Lake and Steep Rock Lake platforms. Ca-carbonate Seas were oxygenated and separated by a chemocline mixing zone from Fe-carbonate Seas that were anoxic and ferruginous. Lines a-d represent equilibrium conditions corresponding to the same lines in Fig. 17.

unlikely that O_2 produced by photolysis in the Archean atmosphere would survive long enough to be effective (Kasting, 1993; Kasting and Brown, 1998; Catling and Claire, 2005). The transformation of Fe^{2+} to ferric hydroxide by ultraviolet radiation also has problems. Experiments suggesting that the reaction does not proceed to produce iron hydroxide led Konhauser et al. (2007a) to conclude that oxide facies in iron formation instead formed by non-photochemical oxidative processes, likely involving oxygenic or anoxygenic photosynthesis.

The possibility has been advanced that Archean and Early Proterozoic oxide facies in iron formations were all originally deposited as greenalite (Rasmussen et al, 2013; Rasmussen and Muhling, 2020, 2021; Rasmussen et al., 2021). In this view, the iron in these iron formations was carried as dissolved Fe^{2+} in hydrothermal plumes and precipitated as greenalite nanoparticles. During deep burial and/or metamorphism the greenalite was replaced by a range of other iron-rich minerals (Rasmussen et al., 2021). Robbins et al. (2019) (see also Stüeken, 2019) summarized arguments against the likelihood of large-scale replacement of greenalite by iron oxides in iron formations, and questioned the duration of the replacement reactions proposed for iron oxide formation in the Hamersley Basin, noting that it appeared that there would have been insufficient time for them to run to completion. In the Mesoarchean sediments studied here, this scenario also does not account for observed increase in the Mn content of the iron formation toward the carbonate platform at Red Lake, reaching 4.1 % MnO_2 (Afroz, 2019), and why there is up to 19 % MnO_2 in the iron formation adjacent to the Steep Rock platform, but <0.5 % MnO_2 further from the carbonate succession (Huston, 1956).

Anoxygenic Fe^{2+} oxidizing phototrophic bacteria employ Fe^{2+} as an electron donor in the conversion of CO_2 and H_2O into organic molecules. This results in iron hydroxides being produced where the bacteria are growing. In contrast oxygenic photosynthesis, conducted for example by cyanobacteria, produces O_2 that diffuses into the environment and can oxidize iron at a distance from the site of oxygen production. If anoxygenic Fe^{2+} phototrophs formed the iron formation they would have had to live on or above the substrate where the iron formation was accumulating, not on the shallower portion of the platform with better light penetration. A possible explanation for this is that the shallow areas were inhabited by cyanobacteria (Kappler et al., 2005), with which the anoxygenic phototrophs could not compete effectively. Kappler et al. (2005) suggested that the anoxygenic phototrophs lived below the mixed surface layer and intercepted the Fe^{2+}-rich water before it reached the cyanobacteria living at shallower depths. However, this would imply that all Archean iron formations formed in deeper water, and it has since become apparent that some were deposited in very shallow coastal areas (Fralick and Pufahl, 2006; Pufahl et al., 2013). Alternatively, if cyanobacteria were not present in the Mesoarchean it is difficult to explain why anoxygenic phototrophs did not live in shallow water with increased light penetration and deposit iron formation there. Additionally, anoxygenic phototrophs depositing iron hydroxide would not have produced: 1) a high Mn zone close to the Steep Rock carbonate platform (Huston, 1956; Fralick and Riding, 2015) and an increase in Mn towards the Red Lake carbonate platform (Afroz, 2015); 2) positive Ce anomalies analyzed in the Red Lake and Steep Rock iron formation samples that indicate Ce precipitation driven by free oxygen and negative Ce anomalies in the carbonates caused by the associated seawater losing Ce in the iron hydroxide precipitation zones (Fralick and Riding, 2015; McIntyre and Fralick, 2017); 3) the $\delta^{98}Mo$ values in Steep Rock and Red Lake carbonate that indicate significant Mn(IV)- and Fe(III)-oxide sequestration of heavy Mo (Thoby et al., 2019).

Conversely, if abundant cyanobacteria were involved in forming the stromatolites in the platform interiors at Steep Rock and Red Lake, they could have generated sufficient free O_2 to create a lateral oxygenation gradient resulting in: 1) significantly greater Mn precipitation closer to the O_2 source; 2) oxidation of Ce^{3+} and precipitation of Ce^{4+} at the redox front where iron formation was being deposited, leading to positive Ce anomalies in the iron formations and negative Ce anomalies in the carbonate inshore from that area, and; 3) creation of the Mn-oxide and light Mo sinks. In this analysis, oxygenic photosynthesis emerges as the only mechanism for iron formation precipitation that is consistent with all currently available data from the Steep Rock and Red Lake Mesoarchean successions. Points 1 and 2 also require O_2 production to have occurred on the carbonate platform. This agrees with the presence of primary aragonite deposits on the outer platform adjacent to the chemocline, whereas calcite precipitation dominated the platform interior. Furthermore, at Steep Rock, a thin (40 cm) bed of laterally linked columnar stromatolites composed of ferroan dolomite (ankerite) is underlain by the only aragonite layer in the platform interior, a 30 cm thick bed of crystal fans. This could record an incursion of Fe^{2+} bearing seawater into the central lagoon that caused a brief transition from calcite precipitation to aragonite precipitation followed by ferroan dolomite (ankerite) precipitation. This, the only sustained incursion of Fe^{2+} bearing seawater into the Steep Rock platform interior so far identified, supports the view that Fe^{2+} content in the seawater constituted a major control on the mineralogy of these carbonate precipitates.

A further possibility is the removal of Fe^{2+} by complexing with phosphate or organics. However, it seems unlikely that P would have had significant impact considering that its concentration in the Archean ocean may have been quite low (Hao et al., 2020), and that high levels of dissolved silica could have interfered with P complexing with Fe^{2+} (Konhauser et al., 2007b). If organic carbon concentrations were sufficiently high to account for precipitation of the iron by organic ligands, then the low amounts of C preserved in the iron formation would have required extensive loss of C by CO_2 generation in the sediment. This should have led to massive dissolution of the iron and its precipitation as siderite, for which there is no evidence.

3.1. Oxygen source

In Archean seas, localized marine oxygenation would have been required to remove sufficient Fe^{2+} from Archean seawater in order to precipitate Ca-carbonate rather than Fe-carbonate (Riding et al., 2014; Fralick & Riding, 2015). If photolysis of H_2O and CO_2 was insufficient to oxygenate the Archean atmosphere (Catling and Claire, 2005), then marine O_2 must have been derived from H_2O during bacterial photosynthesis, enzymatically mediated by photosystem II (Canfield, 2005, Holland, 2006), as proposed by Cloud (1968): '*photosynthesis is the likely process whereby oxygen might eventually appear and be generated fast enough to oxidize most of the reduced substances of the hydrosphere, atmosphere, and surface of the earth and begin to accumulate as a free gas*'. In oxygenic photosynthesis, photosystem II uses light to oxidize water to O_2. At the present day, cyanobacteria are the only prokaryotes known to utilize this system (Oliver et al., 2021). Present-day shallow-water marine stromatolites have long been known to contain cyanobacteria (e.g., Black, 1933; Logan, 1961) and many ~ 3.5–2.8 Ga Ca-carbonate units, including Red Lake and Steep Rock Lake, contain stromatolites (Schopf, 2006). Although cyanobacterial fossils have not been confirmed prior to the Proterozoic (Hofmann, 1976; Demoulin et al., 2019), sheath-like fossils such as *Siphonophycus* could suggest their presence in ~ 3.51 Ga Pilbara sediments (Schopf, 2006) and filamentous mats similar to those formed by cyanobacteria are well-preserved in the ~ 3.475–3.250 Ga Moodies Group of the Barberton Greenstone Belt (e.g., Homann, 2019). It is therefore plausible that oxygenic photosynthesis was extant ~ 3.51 Ga (Walter, 1983; Awramik, 1992; Buick, 2008; Harnmeijer, 2010, p. 316; Planavsky et al., 2014; Ossa Ossa et al., 2018; Wang et al., 2020) and could have facilitated the formation of Archean marine Ca-carbonate platforms such as those at Red Lake and Steep Rock Lake (Riding et al., 2014).

3.2. Observed mineral layering

Although deposits at the seaward margins of both of these carbonate platforms are essentially composed of Ca-carbonate interlayered with

Fe-minerals (Fe-carbonates, Fe-oxides), at Red Lake they appear to be water-column precipitates, whereas at Steep Rock Lake they appear to be essentially seafloor crusts. These contrasting examples provide insight into the conditions interpreted here as platform margin chemocline mixing zones between anoxic Fe-rich offshore and Fe-poor oxygenated onshore seawater (see Fig. 14 for a conceptual model).

3.2.1. *Seafloor-crust interlayering*

At Steep Rock Lake, interlayered Ca-carbonate and Fe-mineral precipitates within the Giant Domes have layer thickness ratios in the range ~ 10:1 to ~ 20:1 (Section 2.2; Figs. 12, 13). We infer that this reflects Fe-carbonate and/or Fe-oxide precipitation (due to oxygenation), followed by precipitation of aragonite crust (due to partial iron removal), and then calcitic cuspate fenestral fabric precipitation (due to virtually complete Fe^{2+} removal). We therefore suggest that these represent seafloor chemocline deposits driven by an oxygenation front. The originally aragonite crust is now calcite but preserves fibrous crystal fabric with abundant Sr that preferentially incorporated into the aragonite (Fig. 15). This deposit also contains negative Ce anomalies indicative of O_2 in seawater (Riding et al., 2014). Fe-carbonate and hematite layers occur between layers of both crystal crust and cuspate fenestral fabric. The cuspate fenestral fabric is calcite and its delicate fabric may represent synsedimentarily lithified microbial films, similar to, but much less well preserved and finer than, those observed in fenestrate microbialite that is locally common in some younger Archean platform carbonates (see Sumner, 1997b). Cuspate fenestral carbonate could broadly be regarded as a type of stromatolite, since it is inferred to be microbial and often appears finely and irregularly layered in outcrop (Fig. 13) and slabs (Fig. 15).

3.2.2. *Fine-grained water-column mineral interlayering*

At Hall Bay, in Red Lake, there is a thin but distinctive horizon intercalated within platform carbonates, described at the end of Section 2.1, which mainly consists of thin alternations of magnetite (with pronounced positive Eu anomalies) and recrystallized calcite (Afroz, 2019) (Fig. 8), together with minor secondary chert horizons (Fig. 16). The calcite was originally probably fine-grained and this horizon of magnetite-calcite layers could reflect water column precipitation within a chemocline located near the platform margin. In this interpretation, mixing of upwelling Fe-rich offshore water with oxygenated onshore water led to Fe^{2+} removal (as Fe-oxide) that then facilitated water-column precipitation of Ca-carbonate mud, either as primary aragonite that was subsequently altered to calcite, or – if O_2 levels were sufficiently high – as primary calcite. The bands of $CaCO_3$ and Fe-oxide layers have overall thickness ratios of ~ 5:1–6:1 (Fig. 8). This ratio is consistent with a larger amount of Fe^{2+} oxidation, and therefore a more offshore location within the chemocline, in comparison to the ~ 10:1–20:1 ratio and more proximal setting of the layered deposits at Steep Rock Lake (Figs. 12, 13).

3.3. *Archean seawater chemistry*

These observations of the rock record support recognition of anoxic and oxygenated water masses separated by a dynamic chemocline (Fig. 14): (i) offshore anoxic iron-rich seawater, precipitating Fe-carbonate and Fe-oxide, (ii) a chemocline mixing zone variously precipitating interlayered calcite, aragonite and iron-rich dolomite, with or without Fe-oxide, where oxygen generated on the carbonate platform caused localized precipitation of oxidized Fe^{3+}, Mn^{4+} and Ce^{4+}, (iii) an onshore iron-poor seawater platform interior precipitating calcite, locally with thin aragonite and ferroan dolomite intercalations deposited during offshore flooding events in an Oxygen Oasis. We used an equilibrium approach based on published estimates of Archean seawater chemistry, together with consideration of kinetic effects of Fe on carbonate minerals, to further analyze these deposits and interpret their formation.

3.3.1. *Published estimates*

Banded iron formation reached peaks of abundance in the late Archean (Konhauser et al., 2017). It typically consists of differing

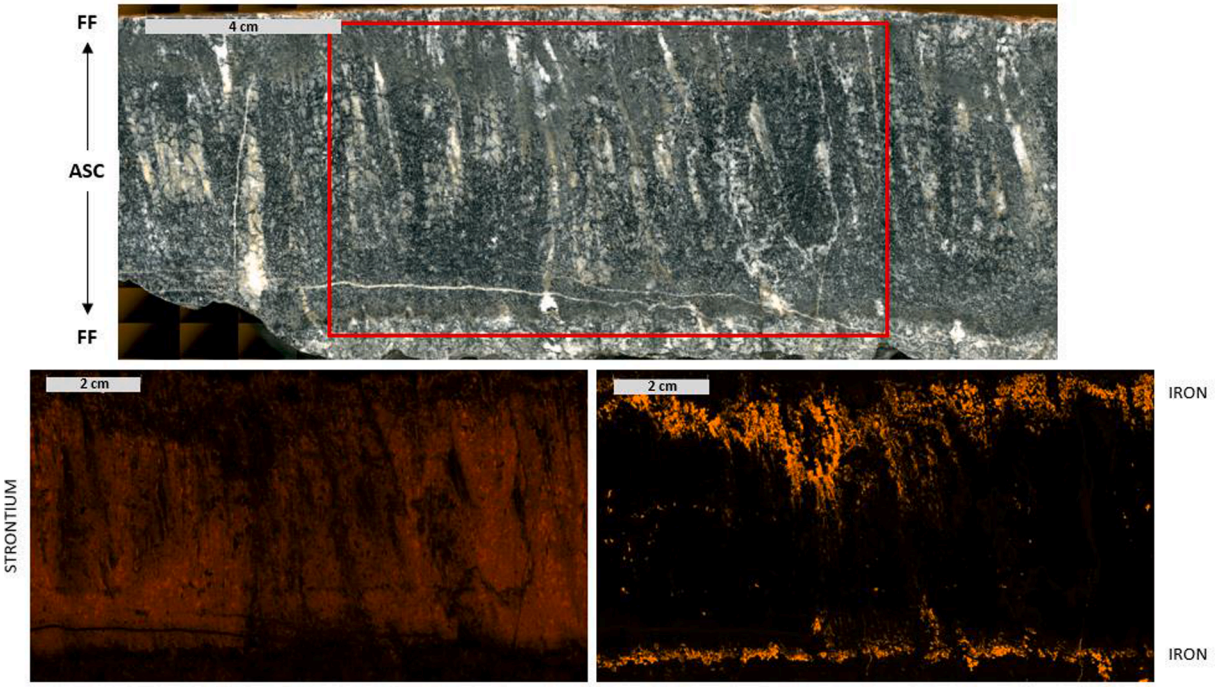

Fig. 15. Steep Rock Lake chemocline precipitates. Vertical polished slab (top) and scans (below) of Steep Rock hybrid dome sample, showing Sr-incorporation (lower left scan) in interpreted primary aragonite seafloor crust (ASC) and Fe-precipitation (lower right scan) at contact with underlying and overlying calcitic Fenestral Fabric (FF). These patterns are consistent with oxidative Fe-removal stimulating rapid aragonite precipitation at a dynamic oxygen-induced chemocline, followed by calcite lithification of microbial mats that colonized the aragonite substrate.

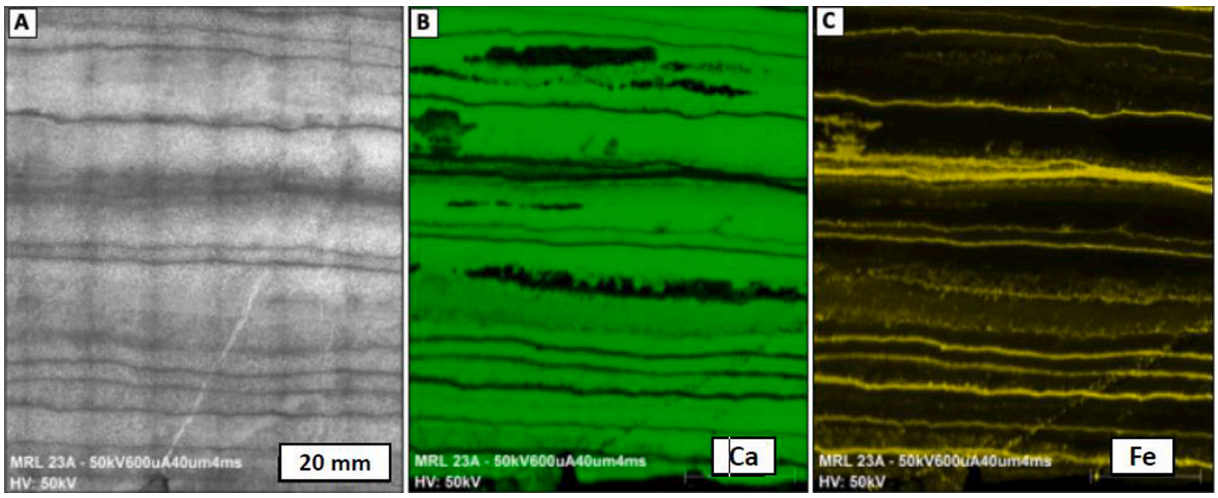

Fig. 16. XRF (X-ray fluorescence) scanned false-color elemental images of intercalated Ca-carbonate and magnetite layers, Hall Bay, Red Lake, Ontario. (A) original image, (B) calcium, (C) iron. Courtesy of M. Afroz (Afroz, 2019, fig. 3.7). Compare Fig. 8.

proportions of silica (chert) and Fe-rich layers, which include iron oxides (hematite, magnetite), Fe-rich silicates (e.g., greenalite, riebeckite, stilpnomelane), and Fe/Mg/Ca carbonates (siderite, ankerite - also termed Fe-dolomite or ferroan dolomite) (James, 1954; Klein and Bricker, 1977; Simonson, 2003; Klein, 2005; Mloszewska et al., 2012; Bekker et al., 2010, 2014; Tosca et al., 2016; Konhauser et al., 2017). These precipitated chemical sediments provide insights into Archean seawater chemistry (Simonson, 2003; Holland, 2005). Despite uncertainties regarding primary phases and minerals, it is widely agreed that the seawater from which iron formation precipitated had significantly elevated dissolved Fe^{2+} and silica (Konhauser et al., 2017) and was essentially anoxic (Canfield, 2005). This does not preclude the existence of localized oxygenated shallow surface and/or marginal zones (MacGregor, 1927; Cloud, 1965; Fischer, 1965; Kasting, 1992; Pavlov and Kasting, 2002; Olson et al., 2013) where iron oxide and/or hydroxide (Holland, 1984; Klein and Beukes, 1989) and Ca carbonates (Klein, 2005; Riding et al., 2014) precipitated. Recent estimates reflect these inferences that Archean seawater was generally Fe rich and O_2 poor (Kipp and Stüeken 2017; Song et al., 2017) (Fig. 1). Reconstructions of Archean seawater pH and temperature, and of atmospheric CO_2 levels, are uncertain. Published estimates for ~ 3.0 Ga include: pH average at 6.83, ranging 6.45–7.44 (Krissansen-Totton, et al., 2018), similar to that of Halevy and Bachan (2017); seawater temperature average 17 °C, ranging 0–35 °C; and average partial pressure of CO_2 (p_{CO2}) at 0.126 atm, ranging 0.0107–0.505 atm (Krissansen-Totton, et al., 2018). There is continuing controversy in the literature concerning these values.

3.3.2. *Seawater chemical equilibrium calculations*

Based on published equilibrium constants and estimates of Archean

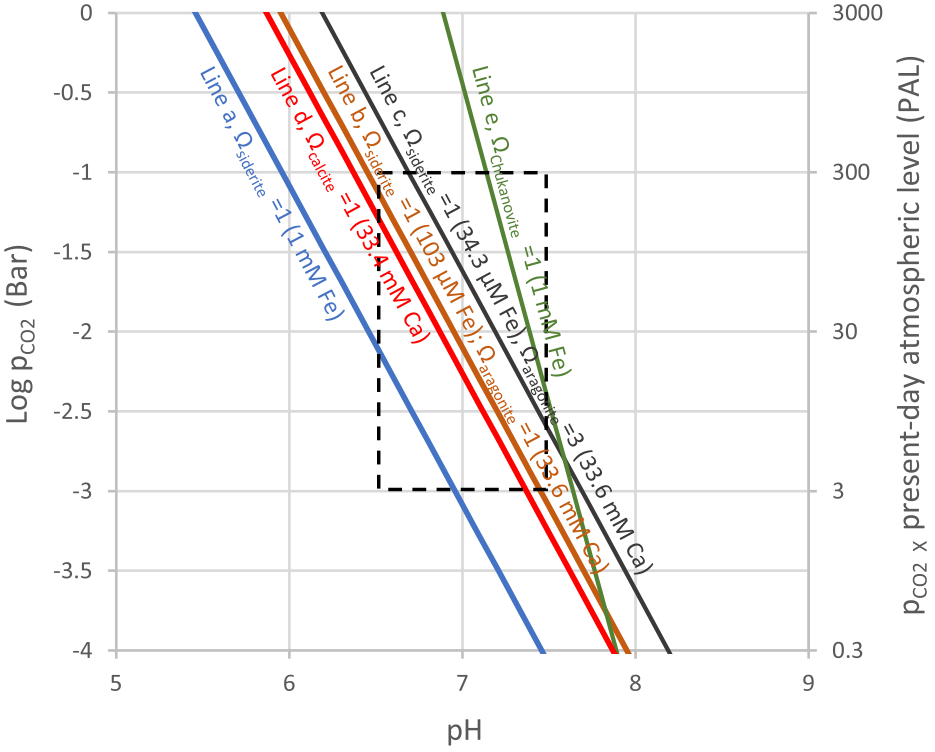

Fig. 17. pH – p_{CO2} stability fields for siderite, aragonite, calcite and chukanovite at 25 °C. Late Archean (~2.9–2.8 Ga) conditions are represented in the dashed black box bounded by pH ranging 6.5–7.5 and p_{CO2} ranging 3–300 × present-day atmospheric level (PAL, where PAL = 350 ppm). Log K_{sp} for siderite, aragonite, calcite, and chukanovite are −10.89, −8.336, −8.48 and 12.42, respectively. Other parameters: seawater salinity = 35 ‰, T = 25 °C, log γ_{Ca} = -0.615 and log γ_{Fe} = -0.657, where γ is ionic activity coefficient. **Line a (blue):** Siderite is at equilibrium with $[Fe^{2+}]$ = 1 mM. Representing basin conditions where siderite is oversaturated at pH and p_{CO2} values above the line. **Line b (brown):** Siderite and aragonite are at equilibrium: $[Ca^{2+}]$ = 33.6 mM, $[Fe^{2+}]$ = 103 µM, representing the chemocline. This also correspond to $\Omega_{siderite}$ = 10 if $[Fe^{2+}]$ = 1 mM. **Line c (black):** $[Fe^{2+}]$ = 34.3 µM, representing the oxidizing side of the chemocline. Calcite is inhibited and $\Omega_{aragonite}$ = 3. **Line d (red):** $[Fe^{2+}]$ = 0 and $[Ca^{2+}]$ = 33.4 mM (0.5 % Ca^{2+} removed) ($\Omega_{aragonite}$ < 1, $\Omega_{calcite}$ = 1), representing platform interior conditions where Fe^{2+} is removed and calcite precipitates. **Line e (green):** Chukanovite is at equilibrium with $[Fe^{2+}]$ = 1 mM.

seawater chemistry (Fig. 1), we constructed a solubility diagram as a function of pH and p_{CO2} for siderite, aragonite, calcite and chukanovite (Fig. 17). The solubility products (log K_{sp}) for siderite, aragonite, and calcite are −10.89, −8.336, and −8.48, respectively (Phreeq C database, Parkhurst and Appelo, 1999). For chukanovite, log K_{sp} is 12.42 for the reaction $Fe_2CO_3(OH)_2 + 3H^+ = 2Fe + HCO_3^- + 2H_2O$ (Kim et al., 2017). We used average present-day seawater salinity, 35 ‰ at a temperature of 25 °C, and the following parameters to represent Archean conditions: 1. For Fe-rich seawater, $[Fe^{2+}] = 1$ mM (Song et al., 2017; Kipp and Stüeken 2017). 2. At siderite and aragonite equilibrium, $[Fe^{2+}] = 103$ μM, given $[Ca^{2+}] = 33.6$ mM (Jones et al., 2015). We note that the siderite and aragonite equilibrium assumption effectively lowers Fe^{2+} from 1 mM to a conservative value, since other ferrous minerals, such as greenalite, chukanovite, would result in higher Fe^{2+} concentrations, and this would require a higher level of oxygen. 3. pH values were in the range 6.5 to 7.5 (Halevy and Bachan, 2017; Krissansen-Totton, et al., 2018). 4. p_{CO2} was in the range 0.001 to 0.1 atm (3 to 300 × present-day atmospheric CO_2 level) (Rosing et al., 2010; Krissansen-Totton et al., 2018). Ionic activity coefficients for Ca and Fe (i.e., log $\gamma_{Ca} = -0.615$ and log $\gamma_{Fe} = -0.657$) were used to convert concentrations to activities in the calculations.

Potential mineral precipitates in equilibrium with the water mass under these conditions are shown by the box in Fig. 17. Thermodynamically, the sequence of expected precipitation occurs from left to right (lines a to e). However, due to the kinetic effect of Fe^{2+} inhibition calcite will not precipitate until Fe^{2+} is removed. *Line a*, calculated with $[Fe^{2+}] = 1$ mM, represents Fe-rich conditions, where siderite is at saturation state, $\Omega_{siderite} = 1$. At pH and p_{CO2} values above the line, siderite is oversaturated, potentially precipitates, and remains stable (see Section 3.5, Fe-Carbonate Sea). *Line b* was constructed assuming that siderite and aragonite were in equilibrium (i.e., $\Omega_{siderite} = 1$ and $\Omega_{aragonite} = 1$), with $[Fe^{2+}] = 103$ μM and $[Ca^{2+}] = 33.6$ mM. The < 1 mM Fe^{2+} could occur by siderite precipitation and/or oxidative removal (i.e., at a chemocline). Alternatively, if the solution contained 1 mM Fe^{2+} then Line b would correspond to $\Omega_{siderite} \sim 10$, indicating that siderite is supersaturated by a factor of 10, while aragonite is at saturation. In this case siderite would precipitate to lower its concentration to 103 μM. *Line c* was constructed assuming $[Fe^{2+}] = 34.3$ μM and $[Ca^{2+}] = 33.6$ mM, resulting in aragonite oversaturation ($\Omega_{aragonite} = 3$). It represents the oxidizing side of a chemocline where O_2 removes some Fe^{2+} ions to form iron oxide. Here, aragonite is expected to precipitate, while calcite is kinetically inhibited by the Fe^{2+} (see Chemocline Mixing Zone in Section 3.5.). *Line d* was constructed assuming 0.5 % Ca^{2+} removal due to aragonite precipitation, resulting in $[Ca^{2+}] = 33.4$ mM, $\Omega_{aragonite} < 1$, $\Omega_{calcite} = 1$; and $[Fe^{2+}] = 0$, i.e., Fe^{2+} is completely removed. This represents platform interior conditions where calcite is expected to precipitate (see Ca-Carbonate Sea in Section 3.5.). *Line e* was calculated with $[Fe^{2+}] = 1$ mM, in equilibrium with chukanovite. Since the Archean seawater conditions (bounded by the box in Fig. 17) are mostly below Line e, chukanovite is undersaturated and would remain in solution. Thus, with respect to the two Fe carbonates, heterogeneous precipitation of siderite is more likely to occur than chukanovite under these conditions.

3.4. Chemocline mineral layering

We suggest that the interlayered Fe-oxide and Ca-carbonate minerals at the platform margins formed when upwelling offshore Fe-rich water mixed with onshore oxygenated shallow water at a chemocline, and that the preserved sediment examples reflect both water column (Red Lake) and seafloor (Steep Rock Lake) precipitation. To analyze these interlayered precipitates, we calculated Ca-carbonate to Fe-oxide thickness ratios as a function of Fe(III) (Fig. 18). At the chemocline, the initial Fe^{2+} and Ca^{2+} concentrations were at 103 μM and 33.6 mM, respectively, assuming that Fe-rich upwelling seawater was in equilibrium with siderite and aragonite, Line b (Fig. 17). We assumed that the onshore water was iron poor ($Fe^{2+} = 0$) and O_2 rich, and that the mixing of these two types of seawater resulted in Fe^{2+} removal in the range 10 to 100 %, and Ca removal of 0.5 % (i.e., ~163 μM, equal to $[CO_3^{2-}]$), as aragonite or calcite.

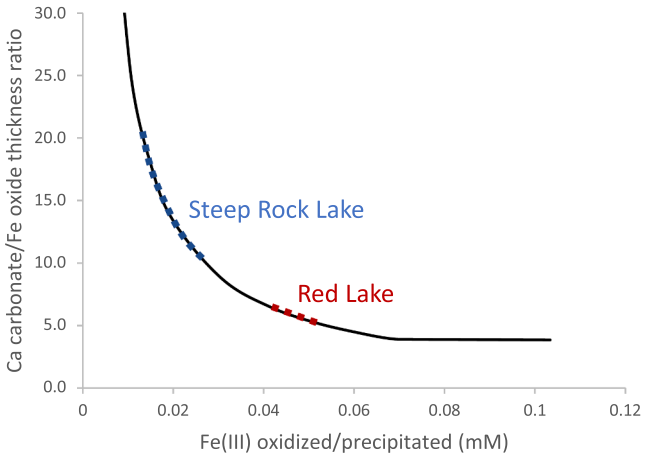

Fig. 18. Estimated thickness ratios of calcium carbonate to iron oxide precipitates, with increasing Fe(III) oxidation at the chemocline. Calculations are based on mixing of anoxic Fe-rich water (containing $[Ca^{2+}] = 33.6$ mM, $[Fe^{2+}] = 103$ μM) with Fe-poor O_2-rich water (containing $[Ca^{2+}] = 33.6$ mM, $[Fe^{2+}] = 0$ μM). This results in Fe(III) precipitation (assumed to be magnetite and hematite). Fe^{2+} removal results in aragonite or calcite precipitation that lowers Ca^{2+} in the final solution by 0.5 % (~163 μM). Blue and red dots indicate carbonate to oxide thickness ratios observed at Steep Rock Lake (~10:1–20:1, see Figs. 12, 13) and Red Lake (~5:1–6:1, see Figs. 8, 16) respectively. (For interpretation of the references to color in this figure legend, the reader is referred to the web version of this article.)

Calculations suggest that, in a mixed solution containing 2.6 to 17.1 μM dissolved O_2, a fraction of the Fe^{2+} would be oxidized, precipitating iron oxide (likely amorphous or poor-crystalline ferrihydrite) with residual Fe^{2+} remaining in solution. No information is available about the rate of Fe^{2+} oxidation at dissolved $O_2 < 6.25$ μM. At 0.2 atm O_2 level (i.e., present-day atmospheric condition) and alkaline pH (~8), Fe^{2+} oxidation, on the order of minutes, is fast (Sung and Morgan, 1980). At low partial pressure of O_2 (0.005 atm), the oxidation rate slows, with a half-life of 40 h (Liang et al., 1993), which is also rapid in terms of geological time. At dissolved $O_2 > 17.1$ μM, stoichiometric oxidation will remove most Fe^{2+}. Fe^{3+} and the remaining Fe^{2+} may form Fe(II)/Fe(III) mixed oxides, such as magnetite. At dissolved O_2 of 25.75 μM, Fe^{2+} is stoichiometrically oxidized, precipitating Fe(III)-oxides, such as hematite. Hematite and magnetite were used in calculating the potentially precipitated oxide minerals. Using these minerals' specific gravities, the mass values were then converted to thickness ratios of calcium carbonate to iron oxide, and plotted as a function of Fe(III) (Fig. 18).

3.4.1. Layer thicknesses

The thin iron-rich layers and thick $CaCO_3$ layers that characterize Steep Rock Domes are consistent with removal of small amounts (<100 μM) of Fe^{2+} followed by precipitation of a larger volume of $CaCO_3$ (Fig. 18). At ~ 300 times higher Ca concentration, the thickness of Ca carbonate could be much greater than observed. However, whereas up to 100 % Fe^{2+} is removed to create the layer thickness, Ca is only removed at ~ 0.5 %, limited by the carbonate in seawater. Density differences between iron oxide minerals and calcium carbonate minerals also affect their relative thickness; for the same mass of precipitation, iron layers will be thinner than Ca-Carbonate layers. The considerable variability observed in the thickness of the Fe and Ca mineral layers is shown in Fig. 18, where high $CaCO_3$ to Fe-oxide mineral thickness ratio corresponds to a low amount of oxidized Fe(III). The proportions of $CaCO_3$ to Fe-oxide minerals (~10:1–20:1, Fig. 12) observed at Steep

Rock are consistent with previously estimated levels of Fe^{2+} in Steep Rock offshore water and of dissolved O_2 in the carbonate platform waters (Riding et al., 2014). In comparison, the $CaCO_3$ to Fe-oxide ratio (~5:1–6:1) observed in interlayered carbonate mud and Fe oxide at Red Lake (Fig. 8) could reflect more Fe-rich water that was further offshore in comparison to the Giant Domes at the Steep Rock margin.

3.4.2. Mineral layer sequences and dynamic chemocline

The ideal sequence of precipitation (i.e., Fe-oxides, aragonite, calcite) consistent with progressive oxidative Fe^{2+} removal is rarely seen in these examples. More commonly, irregular vertical successions of mineral layers are observed in both Steep Rock Giant Domes (Figs. 12 & 13) and Red Lake deposits (Fig. 8). This could reflect dynamic chemocline conditions in which pulses of upwelling offshore seawater mixed, at varying rate, with variably oxygenated onshore seawater. Thus, the vertical succession of mineral layers (Figs. 8, 12, 13) is consistent with lateral changes linked to variations in water composition and flux, underscoring the likely presence of a temporally dynamic chemocline with seasonal/annual or storm induced variability. In addition to the primary iron oxide layers, replacement reactions involving Si, Fe and Mg are important in forming chert, Fe-rich carbonate and iron oxides.

3.5. Two carbonate seas separated by a chemocline mixing zone

Based on the marine sedimentary record in the field areas (Section 2) and inferred Archean seawater chemistry (Section 3.3, Fig. 17), we distinguish two co-existing water masses ~ 2.9–2.8 Ga: (i) anoxic Fe-rich Fe-Carbonate Sea, (ii) oxygenated Fe-poor Ca-Carbonate Sea dominantly precipitating calcite. These were separated by a relatively narrow mixing zone located at a chemocline in which dissolved Fe^{2+} levels were often sufficiently high to inhibit calcite, allowing aragonite to precipitate (Fig. 14). We infer that these water masses reflect the effects of Fe on carbonate precipitation during the rise and expansion of localized marine oxygenation. They likely were present from at least the commencement of the relatively well-preserved carbonate record, ~3.51 Ga (see Section 3.8).

3.5.1. Fe-Carbonate Sea

The two common $CaCO_3$ minerals, calcite and aragonite, are two orders of magnitude more soluble than $FeCO_3$. Consequently, in Archean anoxic seawater with an estimated 1 mM Fe^{2+} (Fig. 1), $FeCO_3$ would precipitate, not $CaCO_3$ (Sumner, 1997a) (Line a, Fig. 17). Fe-carbonate precipitation could have been a significant sink for Fe^{2+} (Tosca et al., 2019). Siderite may have precipitated directly, as has been inferred at Wawa (Garcia et al., 2016), or may have formed during early diagenesis from amorphous Fe carbonate. Homogeneous precipitation of siderite is difficult. With sufficiently high pH (>7.2) amorphous Fe(II) carbonate might form, providing seeds for siderite and chukanovite precipitation (Tosca et al., 2019). Another potential metastable precursor is carbonate green rust (e.g., Halevy et al., 2017). From a carbonate perspective, we regard Archean anoxic seawater as *Fe-Carbonate Seas* (Fig. 14).

3.5.2. Ca-Carbonate Sea

In carbonate platform interiors, we suggest that it is likely that photosynthetic O_2 production removed Fe^{2+}, creating Fe-poor, O_2-rich oases. The absence of Fe allowed $CaCO_3$ precipitation which, depending upon Mg/Ca could have constituted 'Aragonite Seas' or 'Calcite Seas'. Overall, Red Lake platform interior consists of early diagenetic dolomite, possibly associated with shoreline gypsum, and grades distally into mainly calcitic offshore deposits (McIntyre and Fralick, 2017). At both Red Lake and Steep Rock Lake the Sr isotopic values have been reset in the dolomite, whereas they have not been reset in the calcite (Satkoski et al., 2017), implying that the dolomite is secondary. Steep Rock Lake platform can be subdivided into interior fine-grained calcitic sediments (with thin aragonite crusts and Fe-carbonate incursion horizons) and a well-defined margin (Elbow Point Member) of stacked aragonite-calcite hybrid Giant Domes (Fralick and Riding, 2015). We term these *Ca-carbonate Seas* (Fig. 14).

3.5.3. Chemocline mixing zone

In the relatively narrow chemocline zone between Fe-carbonate and Ca-carbonate Seas, oxidation of Fe^{2+} during mixing of anoxic Fe-rich and oxygenated Fe-poor waters would precipitate Fe-oxide and initiate $CaCO_3$ precipitation, due to the availability of CO_3^{2-} that otherwise would have been consumed by $FeCO_3$. Lowering of Fe^{2+} would initially precipitate aragonite, and further Fe^{2+} removal would allow calcite precipitation (Lines b & c, Fig. 17) (Herzog et al., 1989, Katz et al., 1993). These processes are consistent with the interlayering of aragonite and calcite with iron oxide observed in Steep Rock Lake Giant Domes (Section 2.2), and with calcite-magnetite interlayering at Red Lake (Fig. 8). We term this a *chemocline mixing zone* (Fig. 14).

3.6. Presence of iron formation and anoxic seawater incursions

The dominating influence of anoxic Fe-rich seas on the redox chemistry of these mid-Archean carbonate platforms is indicated by the persistent presence of oxide-facies iron formation underlying, intercalated with, and overlying Red Lake carbonates (Sanborn-Barrie et al., 2004; Afroz, 2019), and by manganiferous to non-manganiferous iron formation overlying Steep Rock Lake carbonates (Wilks and Nisbet, 1988; Fralick et al., 2008; Riding et al., 2014; Fralick and Riding, 2015). In addition, a variety of banded sediments suggest relatively short-lived but extensive incursions of anoxic Fe-rich seawater into the platform interiors, presumably offshore-derived and driven by episodic storm and other events. Examples at Red Lake include iron formation intercalations (Afroz, 2019) and the presence of large domes interpreted as originally aragonite (Fig. 4). Thinner, but common, examples at Red Lake and Steep Rock Lake include layers of Fe-dolomite (Fig. 11), herringbone calcite (Fig. 5) (Fralick and Riding, 2015, p. 164) (whose precipitation at Campbellrand has been linked to Fe-influence; Sumner and Grotzinger, 1996a; Sumner, 1997a), and atikokania crystals (Figs. 3, 11) (probably originally aragonite) associated with siderite and Fe-dolomite (see Section 2.2). At Steep Rock, repetitive calcite/Fe-dolomite banding of nearshore stromatolites suggests episodic synsedimentary replacement of Ca-carbonate (aragonite or calcite) by Fe-dolomite during the inception of platform development (Fig. 10). We interpret these well-defined, laterally continuous, closely spaced alternations to reflect oxygenation-related fluctuations in seawater Fe^{2+} concentration that alternately facilitated calcite (more oxygen) and Fe-dolomite (less oxygen) precipitation, although the Fe-dolomite is likely a synsedimentary seafloor replacement of Ca-carbonate, rather than a direct precipitate. In this view, these compositional bands suggest fluctuations in seawater Fe^{2+} in nearshore conditions during the initial stages of carbonate sedimentation, before dissolved O_2 levels became stabilized by expansion of the platform interior water mass. It is unlikely that the bands reflect alteration by fluids moving laterally through the sediment because: 1) the alternating layers in the stromatolites show no sign of having had permeability contrasts, 2) many alteration layers have sharp tops and irregular bottoms suggesting alteration that migrated downward from an upper surface at the water/sediment interface, 3) small-scale fabrics interpreted as water escape structures locally displacing blocks of altered carbonate layers indicate that alteration was very early, predating dewatering. These intercalations are consistent with the notion that the Fe-poor, oxygenated seawater from which these Ca-carbonate platforms precipitated was coeval and confluent with offshore long-lived, Fe-rich, anoxic seas (Fig. 14).

3.7. Chemocline geometry

These results support the earlier suggestion that Steep Rock Giant Dome fabrics "*could have been produced at a shelf margin adjacent to a redox chemocline between oxygenated shelf waters and suboxic, iron-rich*

offshore/basinal waters" (Fralick & Riding, 2015). Recognition of Ca-carbonate chemocline precipitates, in the form of seafloor crusts at Steep Rock Lake and water column precipitates at Red Lake, raises questions concerning overall chemocline geometry. The apparent scarcity of Ca-carbonate minerals in Archean iron formation (Bekker et al., 2010) could suggest that the chemoclines delimiting early carbonate platforms ~ 2.8 Ga were mainly steeply angled and did not generally extend far offshore. In this case, it might be expected that, over time, the oxygen-induced chemocline – although likely often ephemeral and unstable over geologic timescales – would tend to extend offshore and deepen, possibly by outward rotation of the chemocline, as oxygenation progressively removed Fe^{2+} from seawater. Alternatively, if Ca-carbonate mud (probably as aragonite) was precipitated in the water column, at a chemocline where shallow oxygenated water overlay deeper anoxic Fe-rich seawater, it could have been altered to siderite or Fe-dolomite by synsedimentary replacement reactions during settling through the water column, and/or on the seafloor, prior to burial. However, we currently have no evidence to support these possibilities in the study areas, since iron carbonate layers are very rare, and Ca-carbonate layers do not appear to be present, in the iron formation.

3.8. Other potential Archean carbonate chemocline deposits

Carbonate precipitation has been related to oxygen-induced chemocline conditions in a number of Archean successions; e.g., ~3.2 Ga Fig Tree Group (Satkoski et al., 2015); 2.63–2.45 Ga Hamersley Group (Morris, 1993); ~2.5 Ga Transvaal Supergroup (Klein & Beukes, 1989; Beukes et al., 1990; Sumner 1997a); as well as more generally (Beukes and Klein, 1992; Grotzinger and Knoll, 1995; Sumner and Grotzinger, 1996b; Grotzinger and James, 2000). Red Lake calcite-magnetite layers (Fig. 8) resemble silicified calcite/dolomite thinly (2–5 mm) interlayered with magnetite (Harnmeijer, 2010, p. 316, fig. 4a-c) in the ~ 3.51 Ga Coucal Formation at Pilbara (Pasek et al., 2013). Despite their thinness (≤32 cm), these latter interlayered magnetite and Ca-carbonate deposits can be traced for up to 5 km (Harnmeijer, 2010, p. 256). They have been interpreted as offshore water column precipitates associated with '*seasonal destratification of a transiently oxidized surface ocean*' (Harnmeijer, 2010, p. 312, fig. 38). At the transition from ~ 2.5 Ga Campbellrand carbonate platform deposits to overlying Kuruman Iron Formation (Beukes, 1987), fenestral fabrics (e.g., netlike, contorted cryptalgalaminae, *Conophyton*) in the upper part of the Reivilo and upper Gamohaan Formation (Beukes 1987; Klein & Beukes, 1989, fig. 4), could represent chemocline precipitates formed during transgression of anoxic Fe-rich waters from which the iron formation precipitated upon encountering dissolved O_2 (Johnson et al., 2003). Such a depositional setting might be broadly comparable with that of the upper Elbow Point Member at Steep Rock Lake.

4. Conclusions

(1) Persistent chemoclines separated oxygenated ~ 2.9–2.8 Ga carbonate platforms at Red Lake and Steep Rock Lake in Canada's western Superior Province, from coeval, offshore, Fe-rich, anoxic water masses. In these redox zones, progressive oxygenation resulted in the precipitation of interlayered Ca carbonate (aragonite, calcite), ankerite, and Fe oxide minerals.

(2) Thermodynamic calculations further constrain published estimates of pH, p_{CO2}, Fe and Ca concentrations for Archean seawater. This supports the interpretation that thickness ratios of interlayered Ca carbonate and Fe mineral bands (Red Lake ~ 5:1–6:1; Steep Rock ~ 10:1–20:1) reflect more Fe-rich seawater at Red Lake in comparison to the Steep Rock margin.

(3) Chemocline sediments include (a) carbonate mud interbedded with Fe-oxide layers, interpreted as water-column precipitates (e.g., ~2.9 Ga Red Lake), and (b) crystal crusts, originally aragonite, interbedded with Fe-carbonate and Fe-oxide, interpreted as seafloor crusts (e.g., ~2.8 Ga Steep Rock Lake). Chemocline geometry and its offshore extension remain undetermined.

(4) Three laterally confluent carbonate water masses co-existed in these depositional systems: (i) offshore, anoxic, Fe-rich, Fe-carbonate Seas, (ii) narrow, mixing zones at platform margin chemoclines, in which dissolved Fe^{2+} levels were low enough to permit aragonite precipitation but sufficient to inhibit calcite, (iii) extensive oxygenated Fe-poor platform interior Ca-carbonate Seas (Oxygen Oases) variously precipitating calcite, aragonite and synsedimentary dolomite.

(5) In the deposits studied, Fe^{2+} at ~ 3 orders of magnitude lower level, supersedes the effect of Mg^{2+} on Ca-carbonate mineralogy. Depending upon Mg/Ca, Fe-poor platform interior waters could have constituted either 'Mg-influenced Aragonite' or 'Calcite Seas'.

(6) Numerous thin intercalations of aragonite crystal crust (atikokania), herringbone calcite and replacive Fe-dolomite in platform interior carbonates suggest short-lived incursions of offshore, anoxic, Fe-rich seawater, possibly driven by large storm events.

(7) Oxygenic photosynthesis was the likely source of the oxygen required to initiate and sustain thick carbonate platform development adjacent to Fe-rich, anoxic, basins.

CRediT authorship contribution statement

Robert Riding: Conceptualization, Investigation, Writing - original draft, Writing - review & editing. **Liyuan Liang:** Conceptualization, Investigation, Writing - original draft, Writing - review & editing. **Philip Fralick:** Conceptualization, Investigation, Writing - original draft, Writing - review & editing.

Declaration of Competing Interest

The authors declare that they have no known competing financial interests or personal relationships that could have appeared to influence the work reported in this paper.

Data availability

Data for the research is available upon request.

Acknowledgements

Munira Afroz kindly allowed us to use Fig. 16. Philip Fralick's research was supported by a Natural Sciences and Engineering Research Council of Canada Discovery Grant. We thank Eva Stüeken and an anonymous reviewer for detailed and perceptive comments that helped us to improve the final manuscript. We are grateful to Frances Westall for expert editorial guidance.

References

Afroz, M. 2019. Sedimentology and geochemistry of the 2.93 Ga basinal facies of the Rd Lake carbonate platform. MSc thesis, Lakehead University, Thunder Bay, Ontario, Canada, 170p.

Awramik, S.M., 1992. The oldest records of photosynthesis. Photosynth. Res. 33, 75–89.

Balthasar, U., Cusack, M., 2015. Aragonite-calcite seas - Quantifying the gray area. Geology 43, 99–102.

Bekker, A., Slack, J.F., Planavsky, N., Krapez, B., Hofmann, A., Konhauser, K.O., Rouxel, O.J., 2010. Iron formation; The sedimentary product of a complex interplay among mantle, tectonic, oceanic, and biospheric processes. Econ. Geol. 105, 467–508.

Bekker, A., Planavsky, N.J., Rasmussen, B., Krapež, B., Hoffman, A., Slack, J.F., Rouxel, O.J., Konhauser, K.O., 2014. Iron Formations: their origins and implications for seawater chemistry. In: Holland, H., Turekian, K. (Eds.), Treatise on Geochemistry, 2nd ed. Elsevier, pp. 561–628.

Beukes, N.J., 1987. Facies relations, depositional environments and diagenesis in a major early Proterozoic stromatolitic carbonate platform to basinal sequence, Campbellrand Subgroup, Transvaal Supergroup, Southern Africa. Sed. Geol. 54, 1–46.

Beukes, N.J., Klein, C., Kaufman, A.J., Hayes, J.M., 1990. Carbonate petrography, kerogen distribution, and carbon and oxygen isotope variations in an Early Proterozoic transition from limestone to iron-formation deposition, Transvaal Supergroup, South Africa. Econ. Geol. 85, 663–690.
Beukes, N.J., Klein, C., 1992. Models for iron-formation deposition. In: Schopf, J.W., Klein, C. (Eds.), The Proterozoic Biosphere. Cambridge University Press, Cambridge, pp. 147–151.
Black, M., 1933. The algal sedimentation of Andros Island Bahamas. Philosophical Transactions of the Royal Society of London. Series B, Biological Sciences 222, 165–192.
Bots, P., Benning, L.G., Rickaby, R.E.M., Shaw, S., 2011. The role of SO4 in the switch from calcite to aragonite seas. Geology 39, 331–334.
Boyd, P.W., Ellwood, M.J., 2010. The biogeochemical cycle of iron in the ocean. Nat. Geosci. 3, 675–682.
Braterman, P.S., Cairns-Smith, A.G., Sloper, R.W., 1983. Photo-oxidation of hydrated Fe^{2} – Significance for banded iron formations. Nature 303, 163–164.
Buick, 2008. When did oxygenic photosynthesis evolve? Phil. Trans. R. Soc. B 363, 2731–2743.
Cairns-Smith, A.G., 1978. Precambrian solution photochemistry, inverse segregation, and banded iron formations. Nature 76, 807–808.
Canfield, D.E., 2005. The early history of atmospheric oxygen: homage to Robert M. Garrels. Annual Rev. Earth Planetary Sci. 33, 1–36.
Catling, D.C., Claire, M.W., 2005. How Earth's atmosphere evolved to an oxic state: A status report. Earth Planet. Sci. Lett. 237, 1–20.
Chilingar, G.V., 1956. Relationship between Ca/Mg ratio and geologic age. Bull. Am. Assoc. Petrol. Geol. 40, 2256–2266.
Cloud Jr, P.E., 1965. Significance of the Gunflint (Precambrian) microflora. Science 148, 27–35.
Cloud Jr., P.E., 1968. Atmospheric and hydrospheric evolution on the primitive Earth: both secular accretion and biological and geochemical processes have affected Earth's volatile envelope. Science 160, 729–736.
Cloud, P.E., 1973. Paleoecological significance of iron-formations. Econ. Geol. 68, 1135–1143.
Corfu, F., Wallace, H., 1986. U-Pb zircon ages for magmatism in the Red Lake greenstone belt, northwestern Ontario. Can. J. Earth Sci. 23, 27–42.
Davis, D.W., Jackson, M.C., 1988. Geochronology of the Lumby Lake greenstone belt: a 3 Ga complex within the Wabigoon subprovince, northwest Ontario. Geol. Soc. Am. Bull. 100, 818–824.
de Baar, H.J.W., de Jong, J.T.M., 2001. Distributions, sources and sinks of iron in seawater. In: Hunter, K.A., Turner, D. (Eds.), The Biogeochemistry of Iron in Seawater. John Wiley & Sons Hoboken, NJ, pp. 123–253.
Demoulin, C.F., Lara, Y.J., Cornet, L., François, C., Baurain, D., Wilmotte, A., Javaux, E. J., 2019. Cyanobacteria evolution: Insight from the fossil record. Free Radical Biology and Medicine. 140 (2019), 206–223. https://doi.org/10.1016/j.freeradbiomed.2019.05.007.
Dymek, R.F., Klein, C., 1988. Chemistry, petrology and origin of banded iron formation lithologies from the 3800 Ma Isua supracrustal belt, west Greenland. Precambr. Res. 39, 247–302.
Fischer, A.G., 1965. Fossils, early life, and atmospheric history. Proc. Natl. Acad. Sci. USA 53, 1205–1215.
Fralick, P., Hollings, P., King, D., 2008. Stratigraphy, geochemistry and depositional environments of Mesoarchean sedimentary in western Superior Province; implications for generation of early crust. In, ed. K.C. Condie and V. Pease, When did Plate Tectonics begin on Planet Earth? Geol. Soc. Am. Spec. Pap. 440, 77–96.
Fralick, P.W., Pufahl, P.K., 2006. Iron formation in Neoarchean deltaic successions and the microbially mediated deposition of transgressive systems tracts. J. Sediment. Res. 76, 1057–1066.
Fralick, P., Riding, R., 2015. Steep Rock Lake: Sedimentology and geochemistry of an Archean carbonate platform. Earth Sci. Rev. 15, 132–175.
Garcia, T.I., Gorton, M.P., Li, H., Wortmann, U.G., Spooner, E.T.C., 2016. The geochemistry of the 2.75 Ga-old Helen Iron Formation, Wawa, Ontario – Insights into iron formation deposition from carbon isotopes and rare earth elements. Precambr. Res. 275, 357–368.
Grotzinger, J.P., James N.P., 2000. Precambrian carbonates: evolution of understanding. In: Grotzinger, J.P. and James N.P. (eds), Carbonate sedimentation and diagenesis in the evolving Precambrian world. SEPM Special Publication 67, 3–20.
Grotzinger, J.P., Knoll, A.H., 1995. Anomalous carbonate precipitates: Is the Precambrian the key to the Permian? Palaios 10, 578–596.
Halevy, I., Alesker, M., Schuster, E.M., Popovitz-Biro, R., Feldman, Y., 2017. A key role for green rust in the Precambrian oceans and the genesis of iron formations. Nat. Geosci. 10, 135–139.
Halevy, I., Bachan, A., 2017. The geologic history of seawater pH. Science 355, 1069–1071.
Hao, J., Knoll, A.H., Huang, F., Schieber, J., Hazen, R.M., Daniel, I., 2020. Cycling phosphorous on the Archean Earth: Part II, Phosperous limitation on primary production in Archean ecosystems. Geochim. Cosmochim. Acta 280, 360–377.
Hardie, L.A., 1996. Secular variation in seawater chemistry: An explanation for the coupled secular variation in the mineralogies of marine limestones and potash evaporites over the past 600 my. Geology 24 (3), 279–283.
Hardie, L.A., 2003. Secular variations in Precambrian seawater chemistry and the timing of Precambrian aragonite seas and calcite seas. Geology 31, 785–788.
Harnmeijer, J., 2010. Squeezing blood from a stone: Inferences into the Life and Depositional Environments of the Early Archaean. In: Astrobiology & Early Earth Evolution, and Earth & Space Sciences. University of Washington, Seattle, Washington, USA, p. 607 pp..
Herzog, R.E., Shi, Q., Patil, J.N., Katz, J.L., 1989. Magnetic water treatment: the effect of iron on calcium carbonate nucleation and growth. Langmuir 5, 861–867.
Hofmann, H.J., 1976. Precambrian microflora, Belcher islands, Canada: significance and systematics. J. Paleontol. 50, 1040–1073.
Hofmann, H.J., Thurston, P.C., and Wallace, H., 1985. Archean stromatolites from Uchi greenstone belt, northwestern Ontario. In: Ayres, L.D., Thurston, P.C., Card, K.D., Weber, W. (Eds.), Evolution of Archean Supracrustal Sequences. Geol. Ass. of Can. Spec. Paper 28, pp. 125–132.
Holland, H.D., 1973. The oceans: a possible source of iron in iron-formations. Econ. Geol. 68, 1169–1172.
Holland, H.D., 1984. The Chemical Evolution of the Atmosphere and Oceans. Princeton University Press, p. 598 pp..
Holland, H.D., 2005. Sedimentary mineral deposits and the evolution of Earth's near-surface environments. Econ. Geol. 100, 1489–1509.
Holland, H.D., 2006. The oxygenation of the atmosphere and oceans. Philos. Trans. R. Soc. B 361, 903–915.
Hollings, P., Wyman, D., 1999. Trace element and Nd-Sm systematics of volcanic and intrusive rocks from the 3 Ga Lumby Lake greenstone belt, Superior Province: evidence for Archean plume-arc interaction. Lithos 46, 189–213.
Hollings, P., Wyman, D., Kerrich, R., 1999. Komatiite-basalt-rhyolite volcanic associations in Northern Superior Province greenstone belts: significance of plume-arc interaction in the generation of the proto continental Superior. Tithos 46, 137–161.
Homann, M., 2019. Earliest life on Earth: evidence from the Barberton Greenstone Belt, South Africa. Earth-Science Rev. 196 (2019), 102888.
Hood, A.v.S., Wallace, M.W., 2018, Neoproterozoic marine carbonates and their paleoceanographic significance: Global and Planetary Change, v. 160, p. 28-45.
Hood, A.S., Wallace, M.W., 2012. Synsedimentary diagenesis in a Cryogenian reef complex: Ubiquitous marine dolomite precipitation. Sed. Geol. 255–256, 56–71.
Horita, J., Zimmermann, H., Holland, H.D., 2002. Chemical evolution of seawater during the Phanerozoic: implications from the record of marine evaporites. Geochim. Cosmochim. Acta 66, 3733–3756.
Huston, W.J., 1956. The Steep Rock Manganiferous Footwall Paint. Queen's University, Kingston, Canada.. MSc Thesis, 76 pp.
James, H.L., 1954. Sedimentary facies of iron-formation. Econ. Geol. 49, 235–293.
Johnson, C.M., Beard, B.L., Beukes, N.J., Klein, C., & O'Leary, J.M. 2003. Ancient geochemical cycling in the Earth as inferred from Fe isotope studies of banded iron formations from the Transvaal Craton. Contributions to Mineralogy and Petrology, 144, 523–547.
Jones, C., Nomosatryo, S., Crowe, S.A., Bjerrum, C.J., Canfield, D.E., 2015. Iron oxides, divalent cations, silica, and the early earth phosphorus crisis. Geology 43, 135–138.
Kappler, A., Pasquero, C., Konhauser, K.O., Newman, D.K., 2005. Deposition of banded iron formations by anoxygenic phototrophic Fe(II)-oxidizing bacteria. Geology 33, 865–868.
Kasting, J.F., 1992. Models relating to Proterozoic atmospheric and oceanic chemistry. In: Schopf, J.W., Klein, C. (Eds.), The Proterozoic Biosphere, a Multidisciplinary Study. Cambridge University Press, Cambridge, UK, pp. 1185–1187.
Kasting, J.F., 1993. Earth's early atmosphere. Science 259, 920–926.
Kasting, J.F., Brown, L.L., 1998. Setting the stage: the early atmosphere as a source of biogenic compounds. In: Brack, A. (Ed.), the Molecular Origins of Life: Assembling the Pieces of the Puzzle. Cambridge University Press, New York, pp. 35–56.
Katz, J.L., Reick, M.R., Herzog, R.E., Parsiegla, K.I., 1993. Calcite Growth Inhibition by Iron. Langmuir 9, 1423–1430.
Kim, S., Marrs, C., Nemer, M., Jang, J.-J.-H., 2017. Solubility model for ferrous iron hydroxide, hibbingite, siderite, and chukanovite in high saline solutions of sodium chloride, sodium sulfate, and sodium carbonate. ACS Earth Space Chemistry 1, 647–663.
Kipp, M.A., Stüeken, E.E., 2017. Biomass recycling and Earth's early phosphorus cycle. Sci. Adv. 3 (11), eaao4795.
Klein, C., 2005. Some Precambrian banded iron-formations (BIFs) from around the world: their age, geologic setting, mineralogy, metamorphism, geochemistry, and origins. Am. Mineral. 90, 1473–1499.
Klein, C., Beukes, N.J., 1989. Geochemistry and sedimentology of a facies transition from limestone to iron-formation deposition in the Early Proterozoic Transvaal Supergroup, South Africa. Econ. Geol. 84, 1733–1774.
Klein, C., Bricker, O.P., 1977. Some aspects of the sedimentary and diagenetic environment of Proterozoic Banded Iron-Formation. Econ. Geol. 72, 1457–1470.
Konhauser, K.O., et al., 2017. Iron formations: A global record of Neoarchaean to Palaeoproterozoic environmental history. Earth Sci. Rev. 172, 140–177.
Konhauser, K.O., Hamade, T., Raiswell, R., Morris, R., Ferris, F., Southam, G., Canfield, D., 2002. Could bacteria have formed the Precambrian banded iron formations? Geology 30, 1079–1082.
Konhauser, K.O., Amskold, L., Lalonde, S.V., Posth, N.R., Kappler, A., Anbar, A., 2007a. Decoupling photochemical Fe(II) oxidation from shallow-water BIF deposition. Earth Planet. Sci. Lett. 258, 87–100.
Konhauser, K.O., Lalonde, S.V., Amskold, L., Holland, H.D., 2007b. Was there really an Archean phosphate crisis? Science 315, 1234.
Krissansen-Totton, J., Arney, G.N., Catling, D.C., 2018. Constraining the climate and ocean pH of the early Earth with a geological carbon cycle model. PNAS 115 (16), 4105–4110.
Kurucz, S., Fralick, P., 2018. Internal fabric of giant domes in the Mesoarchean Steep Rock carbonate platform, Superior Province, Canada. Canadian Journal of Earth Science. J. Earth Sci. 55, 343–355.
Langford, F.F., Morin, J.A., 1976. The development of the Superior Province of northwestern Ontario by merging island arcs. Am. J. Sci. 276, 1023–1034.

Lebrato, M., et al., 2020. Global variability in seawater Mg: Ca and Sr: Ca ratios in the modern ocean. Proc. Natl. Acad. Sci. 117, 22281–22292.
Liang, L., McNabb, J.A., Paulk, J.M., Gu, B., McCarthy, J.F., 1993. Kinetics of Fe(II) oxygenation at low partial pressure of oxygen in the presence of natural organic matter. Environ. Sci. Technol. 27 (9), 1864–1870.
Lippmann, F., 1973. Sedimentary carbonate minerals. Springer-Verlag, Berlin.
Logan, B.W., 1961. Cryptozoon and associated stromatolites from the Recent, Shark Bay, Western Australia. J. Geol. 69, 517–533.
Lowenstein, T.K., Kendall, B., and Anbar, A.D., 2014, Chapter 8.21, The geologic history of seawater, in Holland, H.D. and Turekian, K.K., eds., The Oceans and Marine Geochemistry: Treatise on Geochemistry, 2nd ed., vol. 8, p. 569–622, Elsevier.
Lowenstein, T.K., Timofeeff, M.N., Brennan, S.T., Hardie, L.A., Demicco, R.V., 2001. Oscillations in Phanerozoic seawater chemistry: evidence from fluid inclusions. Science 294 (5544), 1086–1088.
MacGregor, A.R., 1927. The problem of the Precambrian atmosphere. S. Afr. J. Sci. 24, 155–172.
McIntyre, T., Fralick, P., 2017. Sedimentology and Geochemistry of the 2930 Ma Red Lake-Wallace Lake Carbonate Platform, Western Superior Province, Canada. The Depositional Record 3, 258–287.
Mloszewska, A., et al., 2012. The composition of Earth's oldest iron formations: The Nuvvuagittuq Supracrustal Belt (Québec, Canada). Earth Planet. Sci. Lett. 317–318, 331–342.
Morris, R.C., 1993. Genetic modelling for banded iron-formation of the Hamersley Group, Pilbara Craton, Western Australia. Precambrian Research 60, 243–286.
Morse, J.W., Arvidson, R.S., Lüttge, A., 2007. Calcium carbonate formation and dissolution. Chem. Rev. 107, 342–381.
Nothdurft, L.D., Webb, G.E., Kamber, B.S., 2004. Rare earth element geochemistry of Late Devonian reefal carbonates, Canning Basin, Western, Australia: conformation of a seawater REE Proxy in ancient limestones. Geochim. Cosmochim. Acta 68, 263–283.
Oliver, T., Sanchez-Baracaldo, P., Larkum, A.W., Rutherford, A.W., Cardona, T., 2021. Time-resolved comparative molecular evolution of oxygenic photosynthesis. BBA-Bioenergetics. 1862 (2021), 148400.
Olson, S.L., Kump, L.R., Kasting, J.F., 2013. Quantifying the areal extent and dissolved oxygen concentrations of Archean oxygen oases. Chem. Geol. 362, 35–43.
Ossa Ossa, F., Hofmann, A., Wille, M., 2018. Aerobic iron and manganese cycling in a redox-stratified Mesoarchean epocantinantal sea. Earth Planet. Sci. Lett. 500, 28–40.
Parkhurst, D.L., Appelo, C.A.J., 1999. User's guide to PHREEQC (version 2) - A computer program for speciation, batch-reaction, one-dimensional transport, and inverse geochemical calculations. Water-Resources, Investigations Report 99-4259, US Geological Survey, Denver, Colorado, 326 pp.
Pasek, M.A., et al., 2013. Evidence for reactive reduced phosphorus species in the early Archean ocean. Proc. Natl. Acad. Sci. 110 (25), 10089–10094.
Pavlov, A.E., Kasting, J.F., 2002. Mass-independent fractionation of sulfur isotopes in Archean sediments: strong evidence for an anoxic Archean atmosphere. Astrobiology 2, 27–41.
Percival, J.A., Skulski, T., Sanborn-Barrie, M., Stott, G.M., Leclair, A.D., Corkery, M.T., Boily, M., 2012. Geology and tectonic evolution of the Superior Province, Canada. In J.A. Percival, F.A. Cook, and R.M. Clowes (eds), Tectonic Styles in Canada: The LITHOPROBE Perspective. Geological Association of Canada, Special Paper 49, pp. 321–378.
Planavsky, N.J., et al., 2014. Evidence for oxygenic photosynthesis half a billion years before the Great Oxidation Event. Nat. Geosci. 7, 283–286.
Pufahl, P.K., Piragno, F., Hiett, E., 2013. Riverine mixing and fluvial iron formation: a new type of Precambrian biochemical sediment. Geology 41, 1235–1238.
Rasmussen, B., Maiar, D.B., Krapez, B., Muhling, J.R., 2013. Iron silicate microgranules as precursor sediments to 2.5 billion-year-old banded iron formation. Geology 41, 435–438.
Rasmussen, B., Muhling, J.R., 2020. Hematite replacement and oxidative overprinting recorded in the 1.88 Ga Gunflint iron formation. Geology 47, 688–692.
Rasmussen, B., Muhling, J.R., 2021. Development of a greenalite-silica shuttle during incursions of hydrothermal vent plumes onto Neoarchean shelf, Hamersley region, Australia. Precambr. Res. 353.
Rasmussen, B., Muhling, J.R., Krapez, B., 2021. Greenalite and its role in the genesis of early Precambrian iron formations - review. Earth-Acience Reviews 217, 1–29.
Riding, R., Fralick, P., Liang, L., Afroz, M., Lalonde, S., Ramsay, B., 2020. Fine-grained carbonates in mid-Archean 'Oxygen Oases': Origins and implications for CO2 level. Goldschmidt 2020, Abstract.
Riding, R., Fralick, P., Liang, L., 2014. Identification of an Archean marine oxygen oasis. Precambr. Res. 251, 232–237.
Riding, R., Virgone, A., 2020. Hybrid Carbonates: in situ abiotic, microbial and skeletal co-precipitates. Earth Sci. Rev. 208 (2020), 103300.
Ries, J.B., 2010. Review: geological and experimental evidence for secular variation in seawater Mg/Ca (calcite-aragonite seas) and its effects on marine biological calcification. Biogeosciences 7, 2795–2849.
Robbins, L.J., Funk, S.P., Flynn, S.L., Warchola, T.J., Li, Z., Lalonde, S.V., Rostron, B.J., Smith, A.J.B., Beukes, N.J., de Kock, H.O., Heaman, L.M., Alessi, D.S., Konhauser, K. O., 2019. Hydrogeological constraints on the formation of Paleoproterozoic banded iron formations. Nat. Geosci. 12, 555–563.
Ronov, A.B., 1968. Probable changes in the composition of sea water during the course of geological time. Sedimentology 10, 25–43.
Rosing, M.T., Bird, D.K., Sleep, N.H., Bjerrum, C.J., 2010. No climate paradox under the faint early Sun. Nature 464, 744–747.
Sanborn-Barrie, M., Skulski, T., Parker, J., Dubé, B., 2000. Integrated regional analysis of the Red Lake greenstone belt and its mineral deposits, western Superior Province, Ontario. Geological Survey of Canada, Current Research, 2000-C18. 16 pp.
Sanborn-Barrie, M., Skulski, T., Parker, J., 2001. 300 millions of years of tectonic history recorded by the Red Lake greenstone belt, western Superior Province, Ontario. Geological Survey of Canada, p. 14 p.. Current Research 2001–C19,.
Sanborn-Barrie, M., Skulski, T., Parker, J., 2004. Geology, Red Lake greenstone belt, western Superior Province, Ontario. Geol. Surv. Canada, Open File 4594.
Sandberg, P.A., 1985. Nonskeletal aragonite and pCO2 in the Phanerozoic and Proterozoic. In Sundquist ET and Broecker WS (eds), The Carbon Cycle and Atmospheric CO2, Natural Variations Archean to Present. Geophysical Monograph 32, pp. 585-594. Washington DC: American Geophysical Union.
Satkoski, A.M., Beukes, N.J., Li, W., Beard, B.L., Johnson, C.M., 2015. A redox-stratified ocean 3.2 billion years ago. Earth Planet. Sci. Lett. 430, 43–53.
Satkoski, A.M., Fralick, P.W., Beard, B.L., Johnson, C.M., 2017. Initiation of modern-style plate tectonics recorded in Mesoarchean marine chemical sediments. Geochim. Cosmochim. Acta 209, 216–232.
Schopf, J.W., 2006. Fossil evidence of Archaean life. Philosophical Transactions of the Royal Society, B 361, 869–885.
Simonson, B.M., 1985. Sedimentological constraints on the origins of Precambrian iron-formations. Geol. Soc. Am. Bull. 96, 244–252.
Simonson, B.M., 2003. Origin and evolution of large Precambrian iron formations. In Chan, M.A., and Archer, A.W., eds., Extreme depositional environments: Mega end members in geologic time: Boulder, Colorado, Geological Society of America Special Paper 370, p. 231–244.
Song, H., Jiang, G., Poulton, S.W., Wignall, P.B., Tong, J., Song, H., An, Z., Chu, D., Tian, L., She, Z., Wang, C., 2017. The onset of widespread marine red beds and the evolution of ferruginous oceans. Nat. Commun. 8, 7 pp. https://doi.org/10.1038/s41467-017-00502-x.
Spencer, R.J. and Hardie, L.A. 1990. Control of seawater composition by mixing of river waters and mid-ocean ridge hydrothermal brines. Fluid-Mineral Interactions: A Tribute to H. P. Eugster. Edited by . J. Spencer and l-Ming Chou. The Geochemical Society, Special Publication No. 2, 409-418.
Stott, G.M., Corkery, M.T., Percival, J.A., Simard, M., Goutier, J., 2010. A revised terrane subdivision of the Superior Province. In Summary of Field Work and Other Activities 2010. Ontario Geological Survey, Open File Report 6260, 20-1–20-10.
Stüeken, E.E., 2019. Ancient rust. Nat. Geosci. 12, 498–499.
Sumner, D.Y., 1997a. Carbonate precipitation and oxygen stratification in Late Archean seawater as deduced from facies and stratigraphy of the Gamohaan and Frisco formations, Transvaal Supergroup, South Africa. Am. J. Sci. 297, 455–487.
Sumner, D.Y., 1997b. Late Archean calcite-microbe interactions; two morphologically distinct microbial communities that affected calcite nucleation differently. Palaios 12, 302–318.
Sumner, D.Y., 2002. Neoarchean carbonates — clues to early life and early ocean chemistry. International Association of Sedimentologists, 16th International Sedimentological Congress, Johannesburg, South Africa, Excursion A6, Field Guide, 1–6 July 2002, p. 24.
Sumner, D.Y., Grotzinger, J.P., 1996a. Herringbone calcite: Petrography and environmental significance. J. Sediment. Res. 66, 419–429.
Sumner, D.Y., Grotzinger, J.P., 1996b. Were the kinetics of calcium carbonate precipitation related to oxygen concentration? Geology 24, 119–122.
Sumner, D.Y., Grotzinger, J.P., 2004. Implications for Neoarchean ocean chemistry from primary carbonate mineralogy of the Campbellrand-Malmani Platform, South Africa. Sedimentology 51, 1273–1299.
Sun, Z., Li, J., Huang, W., Dong, H., Little, C.T.S., Li, J., 2015. Generation of hydrothermal Fe-Si oxyhydroxide deposit on the Southwest Indian Ridge and its implication for the origin of ancient banded iron formations. J. Geophys. Res. Biogeosci. 120, 187–203. https://doi.org/10.1002/2014JG002764.
Sung, W., Morgan, J.J., 1980. Kinetics and product of ferrous iron oxygenation in aqueous systems. Environ. Sci. Technol. 14, 561–568.
Thoby, M., et al., 2019. Global importance of oxic molybdenum sinks prior to 2.6 Ga revealed by the Mo isotope composition of Precambrian carbonates. Geology 47 (6), 559–562.
Thompson, K.J., et al., 2019. Photoferrotrophy, deposition of banded iron formations, and methane production in Archean oceans. Sci. Adv. https://doi.org/10.1126/sciadv.aav2869.
Thurston, P.C., 2015. Igneous rock associations 19. Greenstone Belts and Granite-Greenstone Terranes: Constraints on the nature of the Archean world. Geosci. Can. 42, 437–484.
Thurston, P.C., Chivers, K.M., 1990. Secular variation in greenstone sequence development emphasizing Superior Province, Canada. Precambr. Res. 46, 21–58.
Thurston, P.C., Osmani, I.A., and Stone, D. 1991. Northwestern Superior Province: Review and terrane analysis; in Geology of Ontario, (ed.) P.C. Thurston, H.R. Williams, R.H. Sutcliffe and G.M. Stott; Ontario Geological Survey Special Volume 4, Pt 1, p. 81-144.
Thurston, P.C., Kamber, B.S., Whitehouse, M., 2012. Archean cherts in banded iron formation: Insight into Neoarchean ocean chemistry and depositional processes. Precambr. Res. 214–215, 227–257.
Tomlinson, K.Y., Hughes, D.J., Thurston, P.C., Hall, R.P., 1999. Plume magmatism and crustal growth at 2.9 to 3.0 Ga in the Steep Rock and Lumby Lake area, western Superior Rrovince. Lithos 46, 103–136.
Tomlinson, K.Y., Davis, D.W., Stone, D., Hart, T.R., 2003. U-Pb age and Nd isotope evidence for Archean terrain development and crustal recycling in the south-central Wabigoon subprovince, Canada. Contrib. Miner. Petrol. 144, 684–702.
Tosca, N., Guggenheim, S., Pufahl, P.K., 2016. An authigenic origin for Precambrian greenalite: Implications for iron formation and the chemistry of ancient seawater. Geol. Soc. Am. Bull. 128, 512–530.
Tosca, N.J., Jiang, C.Z., Rasmussen, B., Muhling, J., 2019. Products of the iron cycle on the early Earth. Free Radical Biol. Med. 140, 138–153.

Veizer, J., Hoefs, J., Lowe, D.R., Thurston, P.C., 1989. Geochemistry of Precambrian carbonates: II. Archean greenstone belts and Archean sea water. Geochimica et Cosmochinica Acta 53, 859–871.
Walter, M.R., 1983. Archean stromatolites: evidence of Earth's earliest benthos. In: Schopf, J.W. (Ed.), Earth's Earliest Biosphere. Princeton University Press, Princeton, NJ, pp. 187–213.
Wang, X., Ossa, O.F., Hofmann, A., Agangi, A., Paprika, D., Planavsky, N.J., 2020. Uranium isotope evidence for Mesoarchean biological oxygen production in shallow marine and continental settings. Earth Planet. Sci. Lett. 551.
Webb, G.E., Kamber, B.S., 2000. Rare earth elements in reefal microbialites: A new shallow seawater proxy. Geochim. Cosmochim. Acta 64, 1557–1565.
Webb, G.E., Nothdurft, L.D., Kamber, B.S., Kloprogge, J.T., Zhaos, J.-X., 2009. Rare earth element geochemistry of scleractinian coral skelton during meteoric diagenesis: a sequence through neomorphism of aragonite to calcite. Sedimentology 56, 1433–1463.
Widdel, S., Schnell, S., Heising, S., Ehrenreich, A., Assmus, B., Schnik, B., 1993. Ferrous iron oxidation by anoxygenic phototrophic bacteria. Nature 362, 8340836.
Wilks, M.E., Nisbet, E.G., 1985. Archaean stromatolites from the Steep Rock Group, northwestern Ontario. Canada. Can. J. Earth Sci. 22, 792–799.
Wilks, M.E., Nisbet, E.G., 1988. Stratigraphy of the Steep Rock Group, northwest Ontario: a major Archaean unconformity and Archaean stromatolites. Can. J. Earth Sci. 25, 370–391.